Evolutionary conserved canonical BMP activity controls cortical neurogenesis

Sonia Najas[1,2], Isabel Pijuan[1,2], Anna Esteve-Codina[3], Susana Usieto[1], Juan D. Martinez[1], An Zwijsen[4], Mariona L. Arbonés[1,2], Elisa Martí[1] and Gwenvael Le Dréau[1,*]

[1] Department of Developmental Biology, Instituto de Biología Molecular de Barcelona, CSIC, Parc Científic de Barcelona, C/ Baldiri Reixac 10-15, 08028 Barcelona, Spain.

[2] Centro de Investigación Biomédica en Red de Enfermedades Raras (CIBERER), Barcelona, Spain.

[3] CNAG-CRG, Centre for Genomic Regulation (CRG), Barcelona Institute of Science and Technology (BIST), Baldiri i Reixac 4, 08028 Barcelona, Spain; Universitat Pompeu Fabra (UPF), Barcelona, Spain.

[4] Department of Cardiovascular Sciences, KU Leuven, Leuven 3000, Belgium.

[*] Corresponding author: gldbmc@ibmb.csic.es

Tel: 34-934034972
Fax: 34-934034979

One sentence summary: SMAD1/5 control cortical neurogenesis

Key words: Bone morphogenetic proteins (BMPs); SMAD transcription factors; cerebral cortex; neurogenesis; cortical projection neurons; radial glial cells; intermediate progenitor cells; YAP.

Word count (main article): 1,517

Summary

Bone morphogenetic proteins (BMPs) are multitasking secreted factors from the Transforming Growth Factor-β (TGF-β) superfamily [1], members of which play crucial roles during amniote development [2,3]. BMPs and their canonical signalling through the SMAD1/5/8 transcription factors are known to play key roles during the early steps of central nervous system (CNS) development, influencing events such as neural induction, neural tube closure and dorsal-ventral patterning [4-7]. However, their contribution to the later stages of amniote CNS formation is much less clear. Here we reveal that SMAD1/5 fulfill an evolutionarily conserved role during cortical neurogenesis. Gain- and loss-of-function experiments in chick embryos show that SMAD1/5 activity supports the self-amplification of cortical radial glial cells (RGCs) and impedes their premature differentiation and exhaustion. Using conditional Smad1/5$^{wt/fl}$;Nestin:Cre$^{+/0}$ (SmadNes) mutant mice, we reveal this role to be evolutionarily conserved in mammals. The sustained reduction in SMAD1/5 activity in mouse RGCs increases the generation of early-born cortical excitatory neurons at the expense of late-born neurons. These SmadNes mutant mice also present microcephaly and overall growth retardation. Genome-wide analysis of the transcriptional changes caused by SMAD1/5 inhibition in cortical RGCs indicates that SMAD1/5 positively regulate the activity of YAP, a master regulator of cell growth and organ size [8]. These findings identify an evolutionarily conserved role for canonical BMP signalling in stem cell maintenance and tissue growth during cortical neurogenesis. We anticipate that the regulation of YAP activity by canonical BMP signalling extends beyond the context of cortical neurogenesis and might be a crucial event regulating growth throughout the CNS and in other tissues.

Main Text

To determine the role of the canonical BMP pathway during cerebral cortex development in amniotes, we focused on SMAD1/5/8. There is increasing evidence that the basic gene regulatory networks, progenitor cell types and cellular events governing the neuron generation during corticogenesis are evolutionarily conserved between mammals and diapsids, particularly birds [9-13]. Thus, we first assessed the role of SMAD1/5/8 in cortical neurogenesis in the chick. The production of neurons in the PAX6$^+$ developing chick cerebral cortex spans from embryonic days (E)3 to E8 [9] (Fig. 1a and Extended Data Fig.1). As in mammals [14], cortical neurogenesis in the chick is initiated by the onset of asymmetric neurogenic divisions of PAX6$^+$;TBR2$^-$ radial glial cells (RGCs) that divide apically in the ventricular zone (VZ, Figs 1a,b and Extended Data Fig.1). From E5 onwards, the production of cortical neurons is enhanced by symmetric neurogenic divisions of basally dividing TBR2$^+$ intermediate progenitor cells [9] (IPCs, Figs 1a,b and Extended Data Fig.1). *In situ* hybridization revealed that both *cSmad1* and *cSmad5* transcripts are expressed throughout this neurogenic period, mostly in the VZ where *cSmad8* transcripts were essentially absent (Extended Data Fig.2). Immunostaining with an antibody that specifically recognizes the active, carboxy-terminal phosphorylated form of SMAD1/5/8 (pSMAD1/5/8) revealed activity of these canonical BMP effectors in both apically- and basally-dividing cortical progenitors as well as in differentiating neurons (Fig. 1c). When quantified in pH3$^+$ mitotic nuclei, SMAD1/5 activity was weaker in basal IPC divisions than in RGC divisions (Fig. 1d). When quantified after *in ovo* electroporation of a pTis21:RFP reporter that is specifically activated during neurogenic divisions [15-17] (Extended Data Fig.3), SMAD1/5 activity was diminished in pTis21:RFP$^+$ neurogenic divisions relative to pTis21:RFP$^-$ self-amplifying divisions (Figs 1e,f). Therefore, a positive correlation

exists between SMAD1/5 activity and the potential for RGC self-amplification during chick cortical neurogenesis.

Endogenous SMAD1/5 activity was inhibited from the onset of cortical neurogenesis by *in ovo* electroporation of sh-RNA plasmids that specifically target *cSmad1* or *cSmad5* (sh-S1/5) [18], which nearly doubled the proportion of electroporated RGCs undergoing neurogenic pTis21:RFP$^+$ divisions (Figs 1g,h). This precocious switch to neurogenic divisions equally caused by either SMAD1 or SMAD5 inhibition provoked a premature depletion of electroporated PAX6$^+$;TBR2$^-$ RGCs, their accelerated progression towards a committed TBR2$^+$ fate and ultimately, their differentiation into SOX2$^-$;HuC/D$^+$ and TBR1$^+$ neurons (Figs 1i,j and Extended Data Fig.4). Conversely, enhancing canonical BMP activity through *in ovo* electroporation of a constitutively active SMAD5 mutant (SMAD5-S/D) [18] produced the opposite phenotype, a 2-fold reduction in the proportion of electroporated RGCs undergoing neurogenic pTis21:RFP$^+$ divisions (Figs 1k,l). This reduction in neurogenic divisions was associated with the electroporated cells remaining as PAX6$^+$;TBR2$^-$ RGCs and it impeded their transition into the neuronal lineage (Figs 1m,n). Notably, the SMAD5-S/D construct rescued the phenotype caused by sh-S5 (Extended Data Fig.5 a,b). In 5 out of 20 electroporated embryos, SMAD5-S/D electroporation itself caused the abnormal generation of ectopic rosettes of cortical progenitors, which developed an apical-basal polarity (Extended Data Fig.5 c). Together, these data identify a new role for SMAD1/5 in regulating cortical neurogenesis during chick development, whereby the fine tuning of SMAD1/5 activity is required to properly balance the maintenance of RGCs with the production of cortical excitatory neurons.

We next assessed whether this function of SMAD1/5 is conserved during neurogenesis in the mammalian cerebral cortex. Unlike *mSmad8*, *mSmad1* and *mSmad5*

transcripts are clearly expressed throughout the rostral-caudal axis of the developing mouse cerebral cortex at E14.5, and they are particularly enriched in the VZ (Fig. 2a). As in chick embryos, pSMAD1/5/8 immunostaining revealed SMAD1/5 activity to be stronger in apically dividing mouse RGCs than in basally dividing IPCs (Figs 2b,c), suggesting a conservation of their role in maintaining cortical RGCs. To further understand the role played by SMAD1/5 during mouse cerebral cortex development, we crossed *Smad1*$^{fl/fl}$*;Smad5*$^{fl/fl}$ mice with a *Nestin:cre* transgenic line that produces Cre-mediated recombination in neural progenitor cells and somites as early as E8.5 [19,20]. Both SMAD1 and SMAD5 protein levels were reduced by ≈50% in E11.5 Smad1$^{wt/fl}$;Smad5$^{wt/fl}$;Nestin:Cre$^{+/0}$ embryos (hereafter referred to as SmadNes mutants or +/-) relative to the control Smad1$^{wt/fl}$;Smad5$^{wt/fl}$;Nestin:Cre$^{0/0}$ littermates (Extended Data Figs 6a,b). The SmadNes mutant mice were viable, born following Mendelian ratios and sterile. From their early postnatal days to adulthood the SmadNes mutants were smaller and ≈30% lighter than their control littermates (Figs 2d,e), revealing severe growth retardation. Interestingly, the SmadNes mutants were microcephalic and while their brain/body weight ratio was higher at P7, it had recovered to normal levels by adulthood (Figs 2f-h), a characteristic reminiscent of human primordial dwarfism syndromes [21]. The size reduction of the adult SmadNes mutant brain was constant across the rostral-caudal axis (Extended Data Figs 6c,d), suggesting that SMAD1/5 inhibition impaired growth equally in all brain regions. Apart from these growth defects and a thinner corpus callosum, the brain of the SmadNes mutants did not present any major neuro-anatomical defects (Fig. 2i and Extended Data Fig. 6e). Intriguingly, the neocortex of adult SmadNes mutants did not appear to have fewer neurons along the radial axis but the relative proportions of its neuronal layers were altered (Figs 2j-m). The number of early-born, NeuN^{+} neurons forming the deep layer L6 and its thickness

increased, whereas these parameters diminished in the superficial L2/3 layer containing late-born callosal projection neurons, consistent with the reduced thickness of the corpus callosum (Figs 2k-m and Extended Data Figs 6c-e). This phenotype was observed at P7 (Extended Data Fig.7), supporting the idea that these cortical defects originated during the embryonic phase of cortical neurogenesis.

While the SmadNes mutant embryos did not present any obvious defect in telencephalic patterning (Extended Data Figs 8a,b), their programme of cortical neurogenesis did appear to be altered (Fig. 3). Around the onset of cortical neurogenesis (E11.5), the SmadNes mutant embryos had correct numbers of cortical RGCs ($PAX6^+$;$TBR2^-$ cells) and IPCs ($TBR2^+$ cells) per radial unit, yet their neuronal output was increased (Figs 3a-f). Accordingly, there were more early-born differentiating $TBR1^+$ neurons in the SmadNes mutant cortex than in their control littermates from E11.5 onwards (Figs 3g,h). The developing cerebral cortex of the SmadNes mutant embryos contained fewer IPCs from E13.5 onwards and fewer RGCs at E17.5 (Figs 3b-d). This decrease in cortical progenitors at E17.5 was associated with a lower neuronal output and fewer late-born $SATB2^+$ neurons (Figs 3e,f and i,j). The mitotic indices of the RGCs and IPCs were comparable in SmadNes mutants and controls at all stages examined (Extended Data Figs 8c-e), indicating that the alterations to cortical neurogenesis in SmadNes mutants are not the result of altered cell cycle kinetics. Together, these data confirmed the developmental origin of the cortical alterations seen in the cerebral cortex of the adult SmadNes mutants (Figs 2k-m). They moreover reveal that mouse cortical progenitors with weaker SMAD1/5 activity prematurely switch to neurogenic divisions, enhancing the generation of early-born cortical neurons and prematurely exhausting the RGC and IPC pools. Consequently, the production of late-

born cortical neurons is limited. As such, the role of SMAD1/5 in promoting stem cell maintenance appears to be conserved in mammalian corticogenesis.

To identify the gene regulatory networks controlled by SMAD1/5 during cortical neurogenesis, cortical RGCs from SmadNes mutant and control E12.5 embryos were purified by FACS based on Prom inin1 expression [22], and their transcriptomas compared by genome-wide RNA-sequencing (Fig. 4a). A short list of differentially expressed transcripts (DETs) was identified (90 DETs with adj $p<0.05$ and 128 with adj $p<0.1$, Fig. 4b and Table S1) and a gene ontology term enrichment analysis correlated this DET signature to the regulation of neurogenesis and cell biosynthesis (Fig. 4c). A Transfac/Jaspar analysis revealed that the promoter regions of these DETs are enriched in binding motifs for transcription factors of the TEAD and SP families (Fig. 4d). The activity of TEADs depend directly on the availability of their co-factors YAP/TAZ [8]. YAP/TAZ are themselves regulated by various upstream signals, including the IGF and Hippo signalling pathways that regulate cell growth and organ size, and the deregulation of which has been linked to primordial dwarfism syndromes [8,21]. Remarkably, SMAD1/5 and YAP may interact physically and act synergistically [23,24]. Therefore, we analysed YAP expression and activity relative to SMAD1/5 activity during cortical neurogenesis. Immunostaining for the YAP protein revealed that the active (nuclear) YAP was more intense in apically-dividing RGCs than in basally-dividing IPCs, strongly correlated with SMAD1/5 activity in both chick and mouse cortical neurogenesis (Extended Data Fig.9). Inhibiting SMAD1/5 during chick cortical neurogenesis impaired YAP activity, as witnessed through the reduced nuclear YAP intensity and the increase in the phosphorylated form of YAP primed for proteasomal degradation (pYAP) relative to the total YAP (Figs 4e-h). Similarly, the pYAP/YAP ratio increased in the cortex of E11.5 SmadNes mutant embryos (Figs 4i,j and Extended

Data Fig.10). These latter findings indicate that SMAD1/5 control YAP activity during cortical neurogenesis, both during mouse and chick development.

Considering this functional cooperation between SMAD1/5 and YAP, the overall reduction in brain size presented by the SmadNes mutant mice and the fact that SMAD1/5 also promote stemness during spinal neurogenesis [15], our results suggest that BMPs and their canonical effectors SMAD1/5 represent master regulators of stem cell maintenance and tissue growth during CNS development.

References

[1] Schmierer, B. & Hill, C.S., TGFbeta-SMAD signal transduction: molecular specificity and functional flexibility. *Nat Rev Mol Cell Biol* 8 (12), 970-982 (2007).

[2] Bragdon, B. *et al.*, Bone morphogenetic proteins: a critical review. *Cell Signal* 23 (4), 609-620 (2011).

[3] Zinski, J., Tajer, B., & Mullins, M.C., TGF-beta Family Signaling in Early Vertebrate Development. *Cold Spring Harb Perspect Biol* 10 (6) (2018).

[4] Bier, E. & De Robertis, E.M., EMBRYO DEVELOPMENT. BMP gradients: A paradigm for morphogen-mediated developmental patterning. *Science* 348 (6242), aaa5838 (2015).

[5] Le Dreau, G. & Marti, E., Dorsal-ventral patterning of the neural tube: a tale of three signals. *Dev Neurobiol* 72 (12), 1471-1481 (2012).

[6] Nikolopoulou, E., Galea, G.L., Rolo, A., Greene, N.D., & Copp, A.J., Neural tube closure: cellular, molecular and biomechanical mechanisms. *Development* 144 (4), 552-566 (2017).

[7] Zagorski, M. *et al.*, Decoding of position in the developing neural tube from antiparallel morphogen gradients. *Science* 356 (6345), 1379-1383 (2017).

[8] Yu, F.X., Zhao, B., & Guan, K.L., Hippo Pathway in Organ Size Control, Tissue Homeostasis, and Cancer. *Cell* 163 (4), 811-828 (2015).

[9] Suzuki, I.K., Kawasaki, T., Gojobori, T., & Hirata, T., The temporal sequence of the mammalian neocortical neurogenetic program drives mediolateral pattern in the chick pallium. *Dev Cell* 22 (4), 863-870 (2012).

[10] Cardenas, A. *et al.*, Evolution of Cortical Neurogenesis in Amniotes Controlled by Robo Signaling Levels. *Cell* 174 (3), 590-606 e521 (2018).

[11] Le Dreau, G. *et al.*, E proteins sharpen neurogenesis by modulating proneural bHLH transcription factors' activity in an E-box-dependent manner. *Elife* 7 (2018).

[12] Nomura, T., Gotoh, H., & Ono, K., Changes in the regulation of cortical neurogenesis contribute to encephalization during amniote brain evolution. *Nat Commun* 4, 2206 (2013).

[13] Yamashita, W. *et al.*, Conserved and divergent functions of Pax6 underlie species-specific neurogenic patterns in the developing amniote brain. *Development* 145 (8) (2018).

[14] Taverna, E., Gotz, M., & Huttner, W.B., The cell biology of neurogenesis: toward an understanding of the development and evolution of the neocortex. *Annu Rev Cell Dev Biol* 30, 465-502 (2014).

[15] Le Dreau, G., Saade, M., Gutierrez-Vallejo, I., & Marti, E., The strength of SMAD1/5 activity determines the mode of stem cell division in the developing spinal cord. *J Cell Biol* 204 (4), 591-605 (2014).

[16] Saade, M., Gonzalez-Gobartt, E., Escalona, R., Usieto, S., & Marti, E., Shh-mediated centrosomal recruitment of PKA promotes symmetric proliferative neuroepithelial cell division. *Nat Cell Biol* 19 (5), 493-503 (2017).

[17] Saade, M. *et al.*, Sonic hedgehog signaling switches the mode of division in the developing nervous system. *Cell Rep* 4 (3), 492-503 (2013).

[18] Le Dreau, G. *et al.*, Canonical BMP7 activity is required for the generation of discrete neuronal populations in the dorsal spinal cord. *Development* 139 (2), 259-268 (2012).

[19] Moya, I.M. *et al.*, Stalk cell phenotype depends on integration of Notch and Smad1/5 signaling cascades. *Dev Cell* 22 (3), 501-514 (2012).
[20] Petersen, P.H., Zou, K., Hwang, J.K., Jan, Y.N., & Zhong, W., Progenitor cell maintenance requires numb and numblike during mouse neurogenesis. *Nature* 419 (6910), 929-934 (2002).
[21] Klingseisen, A. & Jackson, A.P., Mechanisms and pathways of growth failure in primordial dwarfism. *Genes Dev* 25 (19), 2011-2024 (2011).
[22] Corti, S. *et al.*, Isolation and characterization of murine neural stem/progenitor cells based on Prominin-1 expression. *Exp Neurol* 205 (2), 547-562 (2007).
[23] Alarcon, C. *et al.*, Nuclear CDKs drive Smad transcriptional activation and turnover in BMP and TGF-beta pathways. *Cell* 139 (4), 757-769 (2009).
[24] Huang, Z. *et al.*, YAP stabilizes SMAD1 and promotes BMP2-induced neocortical astrocytic differentiation. *Development* 143 (13), 2398-2409 (2016).

Acknowledgments

Acknowledgements: we thank the members of M.L.A's and E.M's laboratories for their discussion of this study. We thank E. Rebollo and the IBMB Molecular Imaging platform, J. Comas and the PCB Flow Cytometry facility, and the CNAG-CRG Sequencing Unit for their assistance. We are grateful to E.J. Robertson for providing the *Smad1*$^{fl/fl}$ mice. **Funding:** the work in M.L.A's and E.M's laboratories was supported by the grants SAF2013-46676-P, SAF2016-77971-R, BFU2016-81887-REDT and BFU2016-77498-P. I.P. received a PhD fellowship from the Spanish Ministry of Economy, Industry and Competitiveness (MINEICO, BES2014-069217). A. E-C was supported by ISCIII (MINEICO, PT17/0009/0019) and the Fondo Europeo de Desarrollo Regional (FEDER). G.L.D. was supported by the AECC (AIO2014). **Author contributions:** Conceptualization: S.N. and G.L.D.; Methodology: S.N., I.P., A.E-C., S.U., J.D.M. and G.L.D.; Investigation: S.N., I.P., A.E-C. and G.L.D.; Resources: A.Z., M.L.A and E.M; Visualization: G.L.D.; Writing - Original Draft: G.L.D.; Funding Acquisition: M.L.A. and E.M.; Supervision: M.L.A., E.M. and G.L.D. **Competing interests:** the authors have no competing financial interests to declare. **Data and materials availability:** All data is available in the main text, extended figures or supplementary information. **Correspondence and requests for materials** should be addressed to G.L.D.

Methods

Animals

Smad1$^{wt/fl}$;Smad5$^{wt/fl}$;Nestin:Cre$^{+/0}$ embryos and postnatal mice were obtained by crossing *Smad1$^{fl/fl}$;Smad5$^{fl/fl}$* mice with transgenic mice that express Cre-recombinase in neural progenitor cells and somites from E8.5 (*NesCre8* mice: 19,20. Smad1$^{wt/fl}$;Smad5$^{wt/fl}$;Nestin:Cre$^{0/0}$ littermates were used as controls. The days of the vaginal plug and birth were defined as E0.5 as P0, respectively. *Smad1$^{fl/fl}$;Smad5$^{fl/fl}$* and *NesCre8* mice were maintained in their original genetic backgrounds. All the experimental procedures were carried out in accordance with the European Union guidelines (Directive 2010/63/EU) and the followed protocols were approved by the ethics committee of the Parc Científic de Barcelona (PCB).

Fertilized white Leghorn chicken eggs were provided by Granja Gibert, rambla Regueral, S/N, 43850 Cambrils, Spain. Eggs were incubated in a humidified atmosphere at 38°C in a Javier Masalles 240N incubator for the appropriate duration and staged according to the method of Hamburger and Hamilton (HH) 25. According to EU animal care guidelines, no IACUC approval was necessary to perform the experiments described herein, considering that the embryos used in this study were always harvested at early stages of embryonic development. Sex was not identified at these stages.

In ovo electroporation

Unilateral *in ovo* electroporations in the developing chick dorsal telencephalon were performed at stage HH18 (E3, 69 hours of incubation). Analyses were performed specifically in the dorsal-medial-lateral (dML) region of the developing chick cerebral cortex to minimize any possible variability along the medial-lateral axis. Plasmids were

diluted in RNAse-free water at the required concentration [0 to 4 µg/µl] and injected into the right cerebral ventricle using a fine glass needle. Electroporation was triggered by applying 5 pulses of 50 ms at 22.5 V with 50 ms intervals using an Intracel Dual Pulse (TSS10) electroporator. Electroporated chicken embryos were incubated back at 38°C and recovered at the times indicated (24-72 hours post-electroporation).

Plasmids

Inhibition of *cSmad1* and *cSmad5* expression was triggered by electroporation of short-hairpin constructs inserted into the pSuper (Oligoengine) or pSHIN vectors together with a control H2B-GFP-producing plasmid as previously reported 11,18,26. Electroporation of 2-4 µg/µl of these constructs caused a specific and reproducible 50% inhibition of the target expression 18. The pCAGGS_SMAD5-SD_ires_GFP, its control pCAGGS_ires_GFP (pCIG), as well as the pTis21:RFP reporter used to assess the modes of divisions undergone by spinal progenitors, were previously described in details 17,18.

In situ hybridization

Chicken embryos were recovered at the indicated stages, fixed overnight at 4ºC in 4% paraformaldehyde (PFA), rinsed in PBS and processed for whole mount RNA *in situ* hybridization following standard procedures. Probes against chick *Smad1* (#chEST899n18) and *Smad8* (#chEST222h17) were purchased from the chicken EST project (UK-HGMP RC). Probe against *cSmad5* was kindly provided by Dr Marian Ros. Hybridized embryos were post-fixed in 4% PFA and washed in PBT. 45µM-thick sections were cut with a vibratome (VT1000S, Leica), mounted and photographed using a microscope (DC300, Leica). The data show representative images obtained from 3

embryos for each stage and probe. The images of *mSmad1, mSmad5 and mSmad8* expression in the developing mouse dorsal telencephalon at E14.5 were obtained from the Genepaint database (https://gp3.mpg.de).

Histology and Immunohistochemistry

Mouse embryos were recovered at the indicated stages and their heads fixed by immersion in 4% PFA for 24 hours at 4ºC, cryoprotected with 30% sucrose in PBS, embedded in Tissue-Tek O.C.T. (Sakura Finetek), frozen in isopentane at -30ºC and sectioned coronally on a cryostat (Leica). Cryosections (14 µm) were collected on Starfrost pre-coated slides (Knittel Glasser) and distributed serially. Postnatal and adult mice were deeply anesthetized in a CO2 chamber and trans-cardially perfused with 4% PFA. The brains were removed, post-fixed and cryoprotected as indicated above and cryotome (40 µm) sections were then distributed serially. Chicken embryos were carefully dissected, fixed for 2 hours at room temperature (RT) in 4% PFA, rinsed in PBS and cryoprotected with 30% sucrose in PBS and 16 µm-thick coronal sections prepared with a cryostat.

For both species, immunostaining was performed following standard procedures. After washing in PBS containing 0.1% Triton X-100 (PBS-0.1% Triton), the sections were blocked for 1 hour at RT in PBS-0.1% Triton supplemented with 10% bovine serum albumin (BSA). When necessary, sections were submitted to an antigen retrieval treatment before blocking by boiling sections for 10 min in sodium citrate buffer (2 mM citric acid monohydrate, 8 mM tri-sodium citrate dihydrate, pH 6.0). For BrdU immunostaining, sections were incubated before blocking in 50% formamide in 2X SSC at 64ºC for 10 min followed by an incubation in 2N HCl at 37ºC for 30 min and finally 10 min in 0.1M boric acid (pH 8.5) at RT. Sections were then incubated overnight at

4ºC with the appropriate primary antibodies (Table S2) diluted in a solution of PBS-0.1% Triton supplemented with 10% BSA or sheep serum. After washing in PBS-0.1% Triton, sections were incubated for 2 hours at RT with the appropriate secondary antibodies diluted in PBS-0.1% Triton supplemented with 10% BSA or sheep serum. Alexa488-, Alexa555- and Cy5-conjugated secondary antibodies were obtained from Invitrogen and Jackson Laboratories. Sections were finally stained with 1 μg/ml DAPI and mounted in Mowiol (Sigma-Aldrich).

Cell cycle exit assay

Pregnant females received an intra-peritoneal injection of BrdU (100 mg/kg; Sigma) and were sacrificed 24 hours later. Embryos were collected and processed as described above. Sections were immunostained for BrdU and Tuj1 and the cell cycle exit rate (neuronal output) was estimated by quantifying the proportion of $BrdU^+$-immunolabelled cells that were $Tuj1^+$ (% of $Tuj1^+$;$BrdU^+$/$BrdU^+$ cells).

Image acquisition and treatment

Optical sections of mouse and chick embryo fixed samples (coronal views) were acquired at RT with the Leica LAS software, in a Leica SP5 confocal microscope using 10x (dry HC PL APO, NA 0.40), 20x (dry HC PL APO, NA 0.70), 40x (oil HCX PL APO, NA 1.25-0.75) or 63x (oil HCX PL APO, NA 1.40-0.60) objective lenses. Maximal projections obtained from 2μm Z-stack images were processed in Photoshop CS5 (Adobe) or ImageJ for image merging, resizing and cell counting. Optical sections of postnatal and adult mouse samples were acquired with a Leica AF7000 motorized wide-field microscope. Cell counting in embryo, postnatal and adult mouse samples were performed in a 100 or 200 μm-wide radial column of the lateral cortical wall, as

indicated in the figures. Cell counts were performed in a minimum of 3 sections of the same rostral-caudal level per embryo or postnatal mouse sample. Quantification of pSMAD1/5/8, PAX6, TBR2, YAP and pYAP intensities was assessed using the ImageJ software. Cell nuclei of mitotic $pH3^+$ cells or $H2B\text{-}GFP^+$ electroporated and neighboring non-electroporated cells were delimitated by polygonal selection, and the mean intensity was quantified as mean gray values.

Western blot

Total protein extracts (≈ 40 μg) were resolved by SDS-PAGE following standard procedures and transferred onto a nitrocellulose membrane (Hybond-ECL, Amersham Biosciences) that was probed with the primary antibodies (Table S2) whose binding was detected by infra-red fluorescence using the LI-COR Odyssey IR Imaging System V3.0 (LI-COR Biosciences).

Purification of mouse Prominin1$^+$ RGCs

The purification of Prominin1$^+$ cortical RGCs was achieved by fluorescence-activated cell sorting (FACS) of dissociated cells obtained from the forebrain of Smad1$^{wt/fl}$;Smad5$^{wt/fl}$;Nestin:Cre$^{+/0}$ and Smad1$^{wt/fl}$;Smad5$^{wt/fl}$;Nestin:Cre$^{0/0}$ E12.5 embryos. Forebrains of littermates with the same genotype were pooled and incubated in Hanks' balanced salt solution (HBSS) containing 0.6% Glucose and 5 mM EDTA for 5 min at 37ºC. Cells were mechanically dissociated by gentle trituration and collected by centrifugation at 300 g for 10 min at 4ºC. Cells were resuspended in 200 µl of incubation media (PBS containing 0.6% glucose, 2% foetal bovine serum and 0.02% NaN_3) and kept for 10 min at 4ºC under soft agitation. Cells were then incubated for 30 min at 4ºC with an APC-conjugated anti-Prominin1 antibody (eBioscience, #17-1331-

81) diluted at 0.2 mg/ml. Incubation with a rat IgG1-APC antibody was performed in parallel to define non-specific fluorescence. After the incubation, cells were centrifuged at 300 g for 10 min at 4ºC and incubated with 1 ml of incubation media. Dissociated cells were then filtered through a falcon tube with a cell strainer cap (BD Biosciences; BD falcon 12 x 75 mm) in which the filter was previously dampened with 500 µl of incubation media. The number of isolated cells was determined using a Neubauer chamber and cells were diluted to a final concentration of 2-3 x 10^6 cells/ml. DAPI (20 ng/mL: Vector Labs) was added to identify dead cells. Sorting was performed with a BD FACS Aria™ Fusion (BD Biosciences) cytometer. After sorting, collector tubes were centrifuged at 1000 g for 10 min at 4ºC and cell pellets stored at -80ºC.

RNA-sequencing

RNA was extracted from pools of 6 x 10^5 FACS-isolated cells using the miRNeasy Micro Kit (Qiagen). Quantification of total RNA was performed by Qubit® RNA BR Assay kit (Thermo Fisher Scientific) and RNA 6000 Nano Bioanalyzer 2100 Assay (Agilent) was used to estimate the total RNA integrity. The 3 pairs of samples of RNAs from SmadNes mutant and control RGCs presenting the best RNA integrity were used for sequencing. Sample preparation protocol for the RNASeq libraries was following the manufacturer's recommendations of KAPA Stranded mRNA-Seq Illumina® Platforms Kit (Roche-Kapa Biosystems). The libraries were sequenced on HiSeq2500 (Illumina) in paired-end mode with a read length of 2x100bp using TruSeq SBS Kit v4 (Illumina). Each sample was sequenced in a fraction of a sequencing v4 flow cell lane, following the manufacturer's protocol. Image analysis, base calling and quality scoring of the run were processed using the manufacturer's software Real Time Analysis (RTA 1.18.66.3) and followed by generation of FASTQ sequence files.

RNA-Seq paired-end reads were mapping against *Mus musculus* reference genome (GRCm38) using STAR version 2.5.3a 27 with ENCODE parameters for long RNA. Isoforms were quantified using RSEM version 1.3.0 28 with default parameters for stranded sequencing and the gencode version M15. Differential isoform analysis was performed with DESeq2 version 1.18 29 with default parameters. We considered differentially expressed transcripts those showing a *p*-adjusted value < 0.05 or *p*-adjusted value <0.1 (extended list). Fold-change (FC) values between genotypes (SmadNes mutants over controls) are expressed in Log2 (Table S1). The GO term enrichment analysis (biologic process) of the extended DET signature was performed with the PANTHER classification system (http://pantherdb.org) and the Transfac/Jaspar analysis using Enrichr 30,31.

Statistical analyses

No statistical method was used to predetermine sample size. The experiments were not randomized. The investigators were not blinded to allocation during experiments. Statistical analyses were performed using the GraphPad Prism 6 software (GraphPad Software, Inc.). Unless noted otherwise (see quantifications), cell counts were typically performed on 3-5 images per embryo and *n* values correspond to different embryos or animals. The normal distribution of the values was assessed by the Shapiro-Wilk normality test. Significance was then assessed with a two-sided unpaired t-test, one-way ANOVA + Tukey's test or two-way ANOVA + Sidak's test for data presenting a normal distribution, or alternatively with the non-parametric Mann–Whitney test for non-normally distributed data. The following convention was used: n.s, non-significant; *P<0.05, **P<0.01, ***P<0.001. The methodology and detailed information related to quantifications are detailed in the following section.

Quantifications

Figs. 1D, 2C: The intensity of endogenous pSMAD1/5/8 immunoreactivity was quantified in mitotic (pH3+) nuclei of apical and basal cortical progenitors obtained from chick E5 (n=5, Fig. 1D) and mouse E13.5 (n=3, Fig. 2C) embryos. The data represent the mean pSMAD1/5/8 intensity ± s.d obtained from 276 apical divisions and 93 basal divisions (Fig. 1D), or 144 apical divisions and 64 basal divisions (Fig. 2C). The dots represent values of individual cells. Significance was assessed with the non-parametric Mann–Whitney test.

Fig. 1F: The intensity of pSMAD1/5/8 immunoreactivity was quantified 24 hours after *in ovo* electroporation of a pTis21:RFP reporter combined to a control plasmid producing H2B-GFP. The data represent the mean pSMAD1/5/8 intensity ± s.d obtained from 107 pTis21:RFP^{+} neurogenic divisions and 137 pTis21:RFP^{-} self-amplifying divisions derived from n=8 electroporated embryos. The dots represent values of individual cells. Significance was assessed with the non-parametric Mann–Whitney test.

Figs 1H, L: The proportion of neurogenic pTis21:RFP^{+} divisions was assessed 24 hours after *in ovo* electroporation of a pTis21:RFP reporter together with sh-S1/S5 (Fig. 1H), SMAD5-S/D (Fig. 1L) or their respective controls. The data represent the mean proportion of neurogenic pTis21:RFP^{+} divisions per embryo ± s.d and show the individual values obtained for each embryo (8-12 embryos per experimental condition). Significance was assessed with the two-sided unpaired t-test.

Figs 1J, N: The proportions of PAX6$^{+/-}$;TBR2$^{+/-}$ and SOX2$^{+/-}$;HuC/D$^{+/-}$ electroporated cells were assessed 48 hours after *in ovo* electroporation with sh-S1/S5 (Fig. 1J), SMAD5-S/D (Fig. 1N) or their respective controls. The data represent the mean proportion ± s.e.m obtained from n embryos as follows: sh-S1/5 (n=12 for PAX6$^{+/-}$;TBR2$^{+/-}$, n=20 for SOX2$^{+/-}$;HuC/D$^{+/-}$) and its control (n=8 for PAX6$^{+/-}$;TBR2$^{+/-}$, n=13 for SOX2$^{+/-}$;HuC/D$^{+/-}$); SMAD5-S/D (n=14 for PAX6$^{+/-}$;TBR2$^{+/-}$, n=15 for SOX2$^{+/-}$;HuC/D$^{+/-}$) and its control (n=10 for PAX6$^{+/-}$;TBR2$^{+/-}$, n=7 for SOX2$^{+/-}$;HuC/D$^{+/-}$). Significance was assessed with a two-way ANOVA + Sidak's test.

Figs 2E, G, H: The body weight (Fig. 2E) and brain weight (Fig. 2G) of SmadNes mutants and control littermates and their body/brain weight ratio (Fig. 2H) were measured at postnatal days P7, P26 and P60. The data represent the mean weight or ratio ± s.d obtained from n embryos per genotype as follows: body weight (Ctrl: n=12 at P7, n=5 at P26 and n=5 at P60; Mutant: n=5 at P7, n=3 at P26 and n=3 at P60), brain weight (Ctrl: n=5 at P7 and n=5 at P60; Mutant: n=2 at P7 and n=3 at P60) and body/brain weight ratio (Ctrl: n=5 at P7 and n=5 at P60; Mutant: n=2 at P7 and n=3 at P60). Significance was assessed with a two-way ANOVA + Sidak's test.

Fig. 2J: The data represent the mean number of NeuN^{+} neurons ± s.d counted in a 100 µm-wide radial column unit of the cerebral cortex of adult SmadNes mutants (n= 3) and control littermates (n= 4). The mean values of individual embryos are shown. Significance was assessed with the non-parametric Mann–Whitney test.

Figs 2L, M: The data represent the mean thickness ± s.e.m (Fig. 2L) and mean number of NeuN^{+} neurons in a 100 µm-wide radial column unit ± s.e.m (Fig. 2M) of the

cerebral cortex of adult SmadNes mutants (n= 3) and control littermates (n= 4). Significance was assessed with a two-way ANOVA + Sidak's test.

Fig. 3C: The data represent the mean number of $PAX6^{+}$;$TBR2^{-}$ (RGCs) cells ± s.d counted in a 100 µm-wide radial column unit of the developing cerebral cortex of SmadNes mutant and control littermates embryos at E11.5 (Ctrl: 5 embryos, Mutant: 5 embryos), E13.5 (Ctrl: 4 embryos, Mutant: 3 embryos) and E17.5 (Ctrl: 4 embryos, Mutant: 4 embryos). The normality was tested using the values of individual sections. The mean values of individual embryos are shown. Significance was assessed with the two-sided unpaired t-test.

Fig. 3D: The data represent the mean number of $TBR2^{+}$ (IPCs) cells ± s.d counted in a 100 µm-wide radial column unit of the developing cerebral cortex of SmadNes mutant and control littermates embryos at E11.5 (Ctrl: 5 embryos, Mutant: 3 embryos), E13.5 (Ctrl: 4 embryos, Mutant: 3 embryos) and E17.5 (Ctrl: 4 embryos, Mutant: 4 embryos). The normality was tested using the values of individual sections. The mean values of individual embryos are shown. Significance was assessed with the two-sided unpaired t-test.

Fig. 3F: The data represent the mean proportion of $Tuj1^{+}$;$BrdU^{+}$/$BrdU^{+}$ cells (neuronal output) ± s.d counted in a 100 µm-wide radial column unit of the developing cerebral cortex of SmadNes mutant and control littermates embryos at E11.5 (Ctrl: 5 embryos, Mutant: 5 embryos), E13.5 (Ctrl: 4 embryos, Mutant: 3 embryos) and E17.5 (Ctrl: 3 embryos, Mutant: 4 embryos). The normality was tested using the values of individual

sections. The mean values of individual embryos are shown. Significance was assessed with the two-sided unpaired t-test.

Fig. 3H: The data represent the mean number of TRB1^{+} neurons ± s.d counted in a 100 µm-wide radial column unit of the developing cerebral cortex of SmadNes mutant and control littermates embryos at E11.5 (Ctrl: 5 embryos, Mutant: 5 embryos), E13.5 (Ctrl: 4 embryos, Mutant: 3 embryos) and E17.5 (Ctrl: 4 embryos, Mutant: 4 embryos). The normality was tested using the values of individual sections. The mean values of individual embryos are shown. Significance was assessed with the two-sided unpaired t-test.

Fig. 3J: The data represent the mean number of SATB2^{+} neurons ± s.d counted in a 100 µm-wide radial column unit of the developing cerebral cortex of SmadNes mutant and control littermates embryos at E17.5 (Ctrl: 5 embryos, Mutant: 3 embryos). The normality was tested using the values of individual sections. The mean values of individual embryos are shown. Significance was assessed with the two-sided unpaired t-test.

Fig. 4F: The intensity of nuclear YAP immunoreactivity was quantified in mitotic pH3^{+}nuclei of H2B-GFP^{+} electroporated and neighboring non-electroporated cells 24 hours after *in ovo* electroporation of sh-S1/S5 or a control plasmid. The data represent the mean ratio of YAP intensity ± s.d quantified in electroporated relative to non-electroporated mitotic cells obtained from n=7 embryos electroporated with sh-S1/S5 (162 pH3^{+};GFP^{+} cells and 140 pH3^{+};GFP^{-} cells) and n=7 embryos electroporated with a control plasmid (147 pH3^{+};GFP^{+} cells and 154 pH3^{+};GFP^{-} cells). The mean values of

individual embryos are shown. Significance was assessed with the non-parametric Mann–Whitney test.

Fig. 4H: The intensities of pYAP and YAP immunoreactivity were quantified in rectangular areas of the developing cerebral cortex of chick embryos 24 hours after *in ovo* electroporation of sh-S1/S5 or a control plasmid. The data represent the mean ratio of pYAP/YAP intensity ± s.d obtained from n=3 embryos electroporated with sh-S1/5 (10 sections) and n=3 embryos electroporated with a control plasmid (7 sections). The dots represent the values of individual sections. Significance was assessed with the non-parametric Mann–Whitney test.

Fig. 4J: The intensities of pYAP and YAP immunoreactivity were quantified in rectangular areas of the developing cerebral cortex of SmadNes mutant and control littermates E11.5 embryos. The data represent the mean ratio of pYAP/YAP intensity ± s.d obtained from n=4 SmadNes mutant (12 sections) and 4 control littermate (12 sections) embryos. The normality was tested using the values of individual sections. The mean values of individual embryos are shown. Significance was assessed with the two-sided unpaired t-test.

Additional References

[25] Hamburger, V. & Hamilton, H.L., A series of normal stages in the development of chick embryo. *J. Morphol.* 88, 49-92 (1951).

[26] Kojima, S., Vignjevic, D., & Borisy, G.G., Improved silencing vector co-expressing GFP and small hairpin RNA. *Biotechniques* 36 (1), 74-79 (2004).

[27] Dobin, A. *et al.*, STAR: ultrafast universal RNA-seq aligner. *Bioinformatics* 29 (1), 15-21 (2013).

[28] Li, B. & Dewey, C.N., RSEM: accurate transcript quantification from RNA-Seq data with or without a reference genome. *BMC Bioinformatics* 12, 323 (2011).

[29] Love, M.I., Huber, W., & Anders, S., Moderated estimation of fold change and dispersion for RNA-seq data with DESeq2. *Genome Biol* 15 (12), 550 (2014).

[30] Chen, E.Y. *et al.*, Enrichr: interactive and collaborative HTML5 gene list enrichment analysis tool. *BMC Bioinformatics* 14, 128 (2013).

[31] Kuleshov, M.V. *et al.*, Enrichr: a comprehensive gene set enrichment analysis web server 2016 update. *Nucleic Acids Res* 44 (W1), W90-97 (2016).

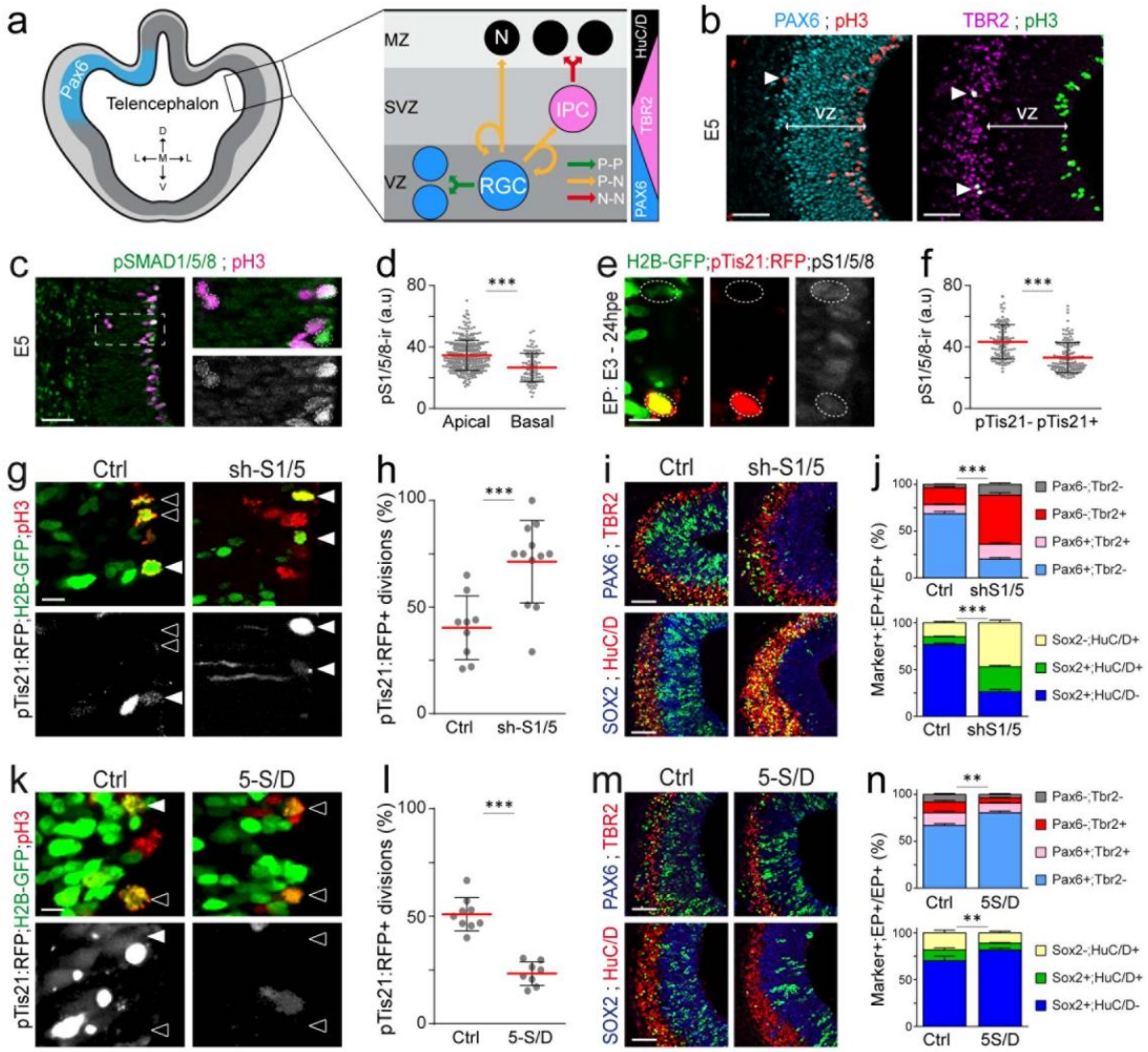

Figure 1: SMAD1/5 promote stem cell maintenance during chick cortical neurogenesis.
a, Cortical neurogenesis in the chick. **b**, Chick PAX6+;TBR2- RGCs and TBR2+ IPCs undergo pH3+ mitoses apically and basally (arrowheads) to the VZ, respectively. **c**, The active, phosphorylated form of SMAD1/5/8 (pSMAD1/5/8) immunoreactivity at E5, and **d**, its quantification in apical and basal mitoses. **e**, The pSMAD1/5/8 immunoreactivity in mitotic cortical progenitors 24 hours after in ovo electroporation (IOE) with the pTis21:RFP reporter along with a control H2B-GFP-producing plasmid, and **f**, its quantification in mitotic pTis21:RFP+ and pTis21:RFP- cortical progenitors. **g-n**, The proportion of electroporated (H2B-GFP+) cortical progenitors undergoing neurogenic pTis21:RFP+ divisions (white arrowheads) after IOE of shRNA plasmids targeting cSmad1 or cSmad5 (sh-S1/5) or their control (**g, h**) or IOE of a constitutively active SMAD5 mutant (5-S/D) or its control (**k, l**). The proportion of PAX6+/-;TBR2+/- and SOX2+/-;HuC/D+/- cells among electroporated (H2B-GFP+) cells 48 hours after IOE of sh-S1/5 (**i, j**), 5-S/D (**m, n**) or their respective controls. *P<0.05, **P<0.01, ***P<0.001. Scale bars: 50 µm (b, c, i, m), 10 µm (e, g, k). VZ: ventricular zone. See also Methods and Extended Data Figs 1-5.

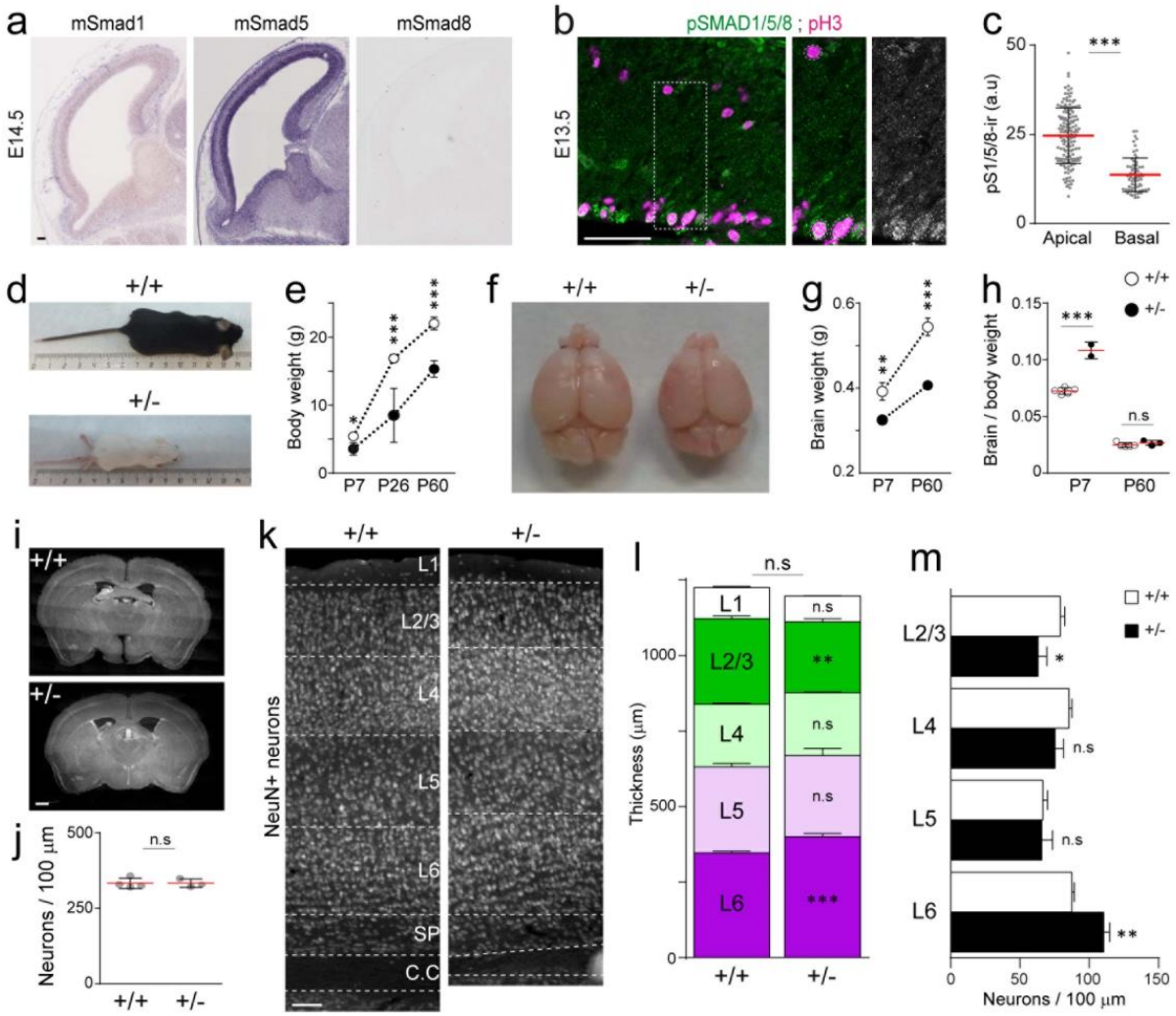

Figure 2: inhibiting SMAD1/5 activity in mouse neural progenitors causes growth retardation, microcephaly and cortical alterations. **a**, The sagittal sections of the developing mouse dorsal telencephalon showing mSmad1, mSmad5 and mSmad8 transcripts at E14.5 were obtained from Genepaint (https://gp3.mpg.de). **b**, The pSMAD1/5/8 immunoreactivity at E13.5 and **c**, its quantification in apical and basal mitotic cortical progenitors. **d-h**, The postnatal evolution of SmadNes mutant mice and their control littermates (**d**) in terms of postnatal weight (**e**), brain development (**f**), brain weight (**g**) and the brain/body weight ratio (**h**). **i**, Coronal sections of the brain of adult SmadNes mutant mice and their control littermates. **j-m**, Total neuron number (**j**), neuronal layer organization (**k**), thickness of the layers (**l**) and the number of neurons in the different layers in radial units (100 µm, **m**) of the mature cerebral cortex of SmadNes mutant mice and their control littermates: *P<0.05, **P<0.01, ***P<0.001. Scale bars, 50 µm (b), 100 µm (a, k), 500 µm (i). See also Methods and Extended Data Figs 6-7.

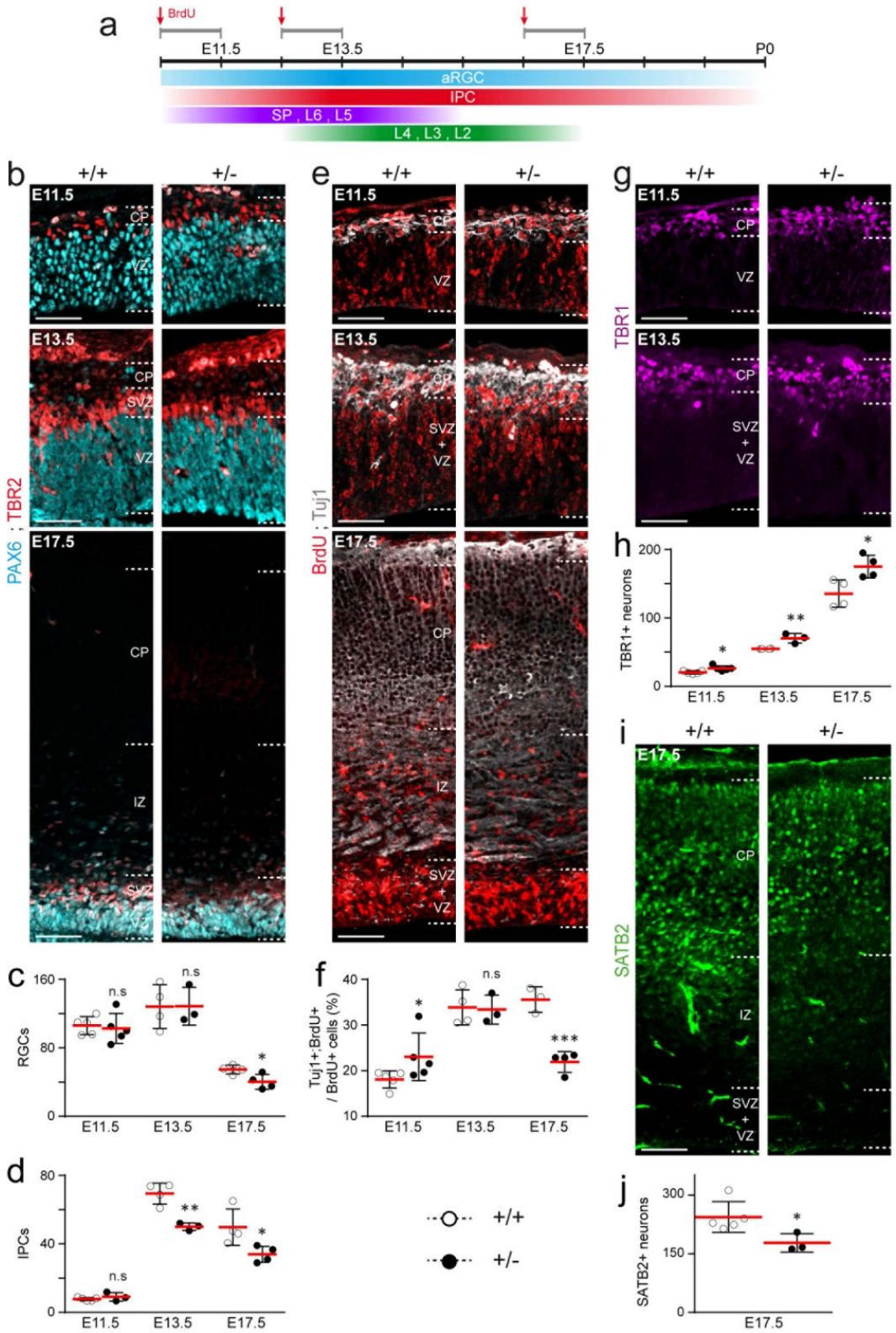

Figure 3: inhibiting SMAD1/5 activity in mouse cortical progenitors causes premature neurogenesis, and depletion of the RGC and IPC pools.

a, Timeline of cortical neurogenesis and BrdU injections during mouse embryonic development. **b-j**, Immunostaining and quantification of PAX6+;TBR2- RGCs and TBR2+ IPCs at early (E11.5), middle (E13.5) and late (E17.5) embryonic stages, indicating the numbers of PAX6+;TBR2- RGCs and TBR2+ IPCs (**b-d**), the neuronal output (% of BrdU+; Tuj1+/BrdU+ cells, **e, f**) and the generation of early-born TBR1+ (**g, h**) and late-born SATB2+ (**i, j**) cortical excitatory neurons quantified per radial unit (100 µm) in the developing cerebral cortex of SmadNes mutant mice and their control littermates during neurogenesis: *P<0.05, **P<0.01,***P<0.01. Scale bars, 50 µm. CP: cortical plate, IZ: intermediate zone, SVZ: sub-ventricular zone, VZ: ventricular zone. See also Methods and Extended Data Fig.8.

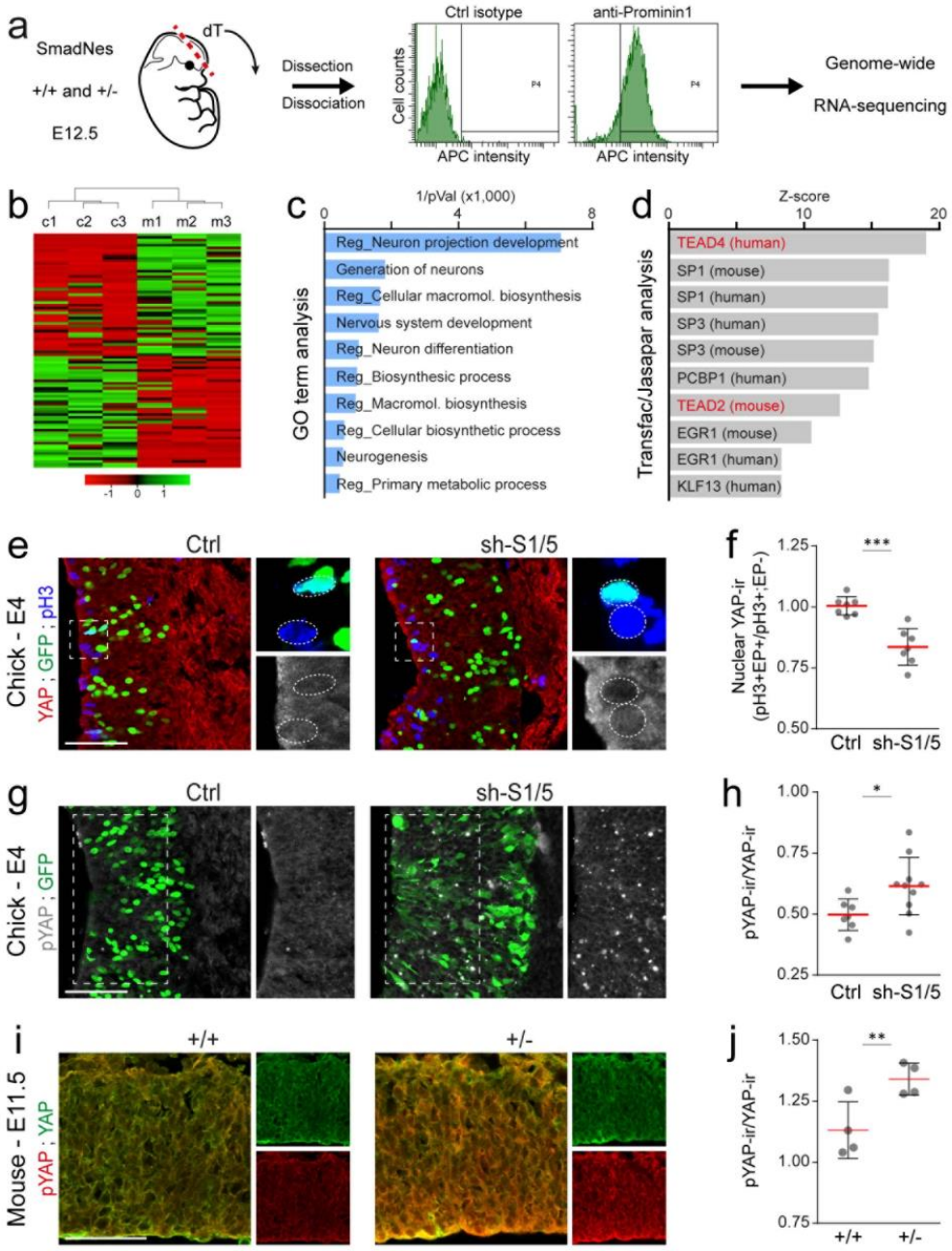

Figure 4: SMAD1/5 regulate YAP activity during early cortical neurogenesis.
a, Comparison of the transcriptome of cortical progenitors from SmadNes mutant and control E12.5 embryos. **b**, Spearman rank correlation and heatmap representing the differentially expressed transcripts (DETs, with a pAdj<0.05) between mutant and control cortical RGCs. **c, d**, Representation of the top 10 gene ontology biological processes (**c**) and transcription factor binding motifs (**d**) associated with the DETs (with a pAdj<0.1). **e**, Immunostaining the developing chick cerebral cortex for total YAP 24 hpe with a control or sh-S1/5 plasmid, and **f**, its quantification in electroporated vs non-electroporated mitotic cortical progenitors. **g,** Immunostaining of pYAP and **h**, quantification of the pYAP/YAP ratio in the developing chick cerebral cortex 24 hpe with control or sh-S1/5 plasmids. **i**, Immunostaining of pYAP and total YAP and **j**, the quantification of the pYAP/YAP ratio in the developing cerebral cortex of E11.5 SmadNes mutant embryos and control littermates: *P<0.05, **P<0.01, ***P<0.001. Scale bars, 50 µm. See also Methods, Extended Data Figs 9-10 and Table S1.

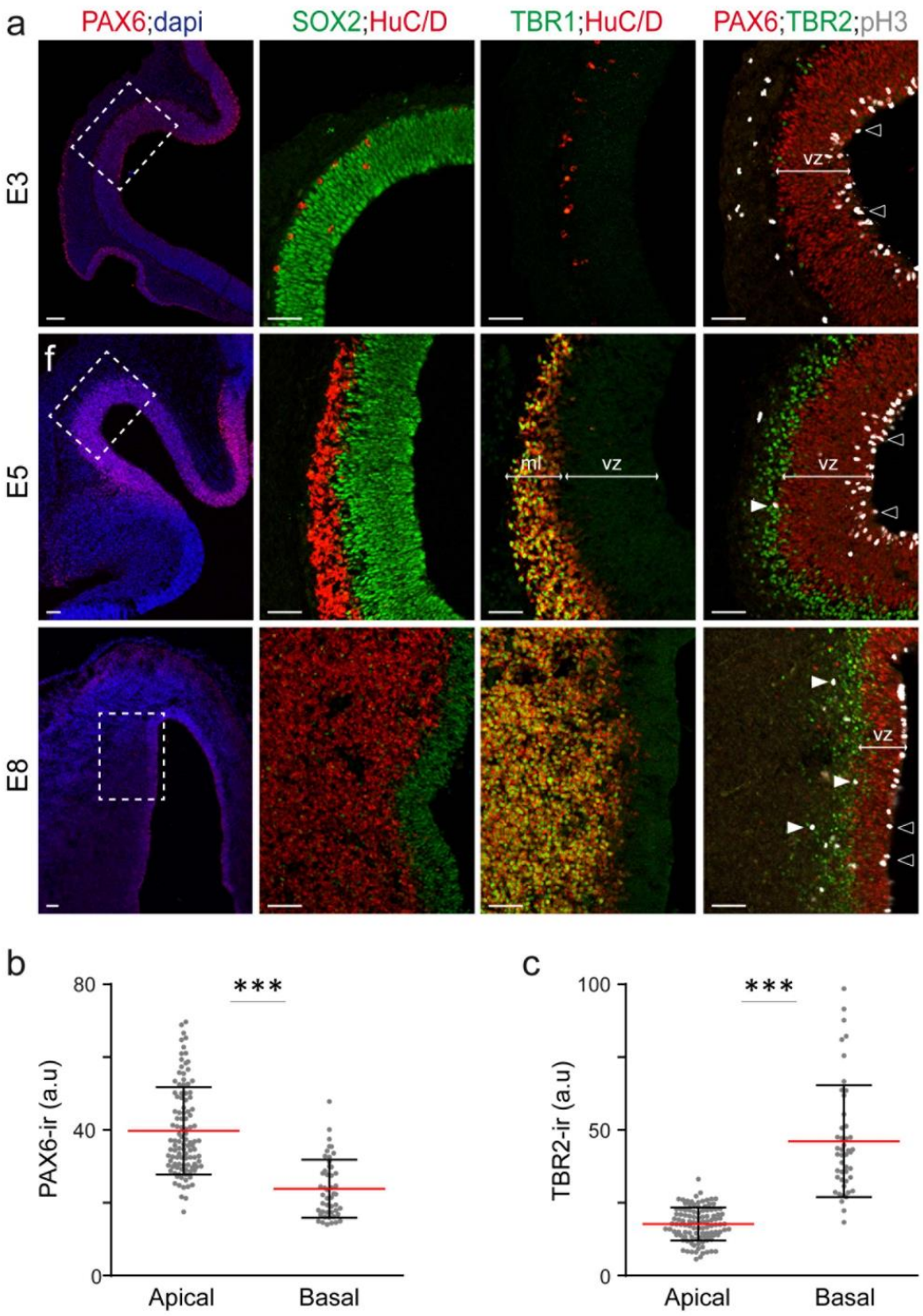

Extended Data Fig.1: Neurogenesis during chick cerebral cortex development.
a, Coronal telencephalic sections from 3, 5 and 8 days-old chick embryos showing the PAX6+ region of the developing chick dorsal pallium. At E3, SOX2+ neural progenitors populate the germinal ventricular zone (VZ) while the first differentiating HuC/D+ neurons migrate basally to form the mantle layer (ML). Neural progenitors from the developing chick cerebral cortex can be subdivided in two different subpopulations: the PAX6+;TBR2- radial glial cells (RGCs) that undergo mitosis at the apical surface (pH3+;PAX6+, black arrowheads) and the TBR2+ intermediate progenitor cells (IPCs) that divide mostly basally from E5 onwards (pH3+;TBR2+, white arrowheads). **b,c**, The intensity of endogenous PAX6 (b) and TBR2 (c) immunoreactivity was quantified in mitotic (pH3+) nuclei of apical and basal cortical progenitors obtained from chick E5 embryos (n=5). The data represent the mean intensity ± s.d obtained from 108 apical divisions and 48 basal divisions. Significance was assessed with the non-parametric Mann–Whitney test.***P<0.001 . Scale bar: 50 µm. VZ: ventricular zone, ML: mantle layer.

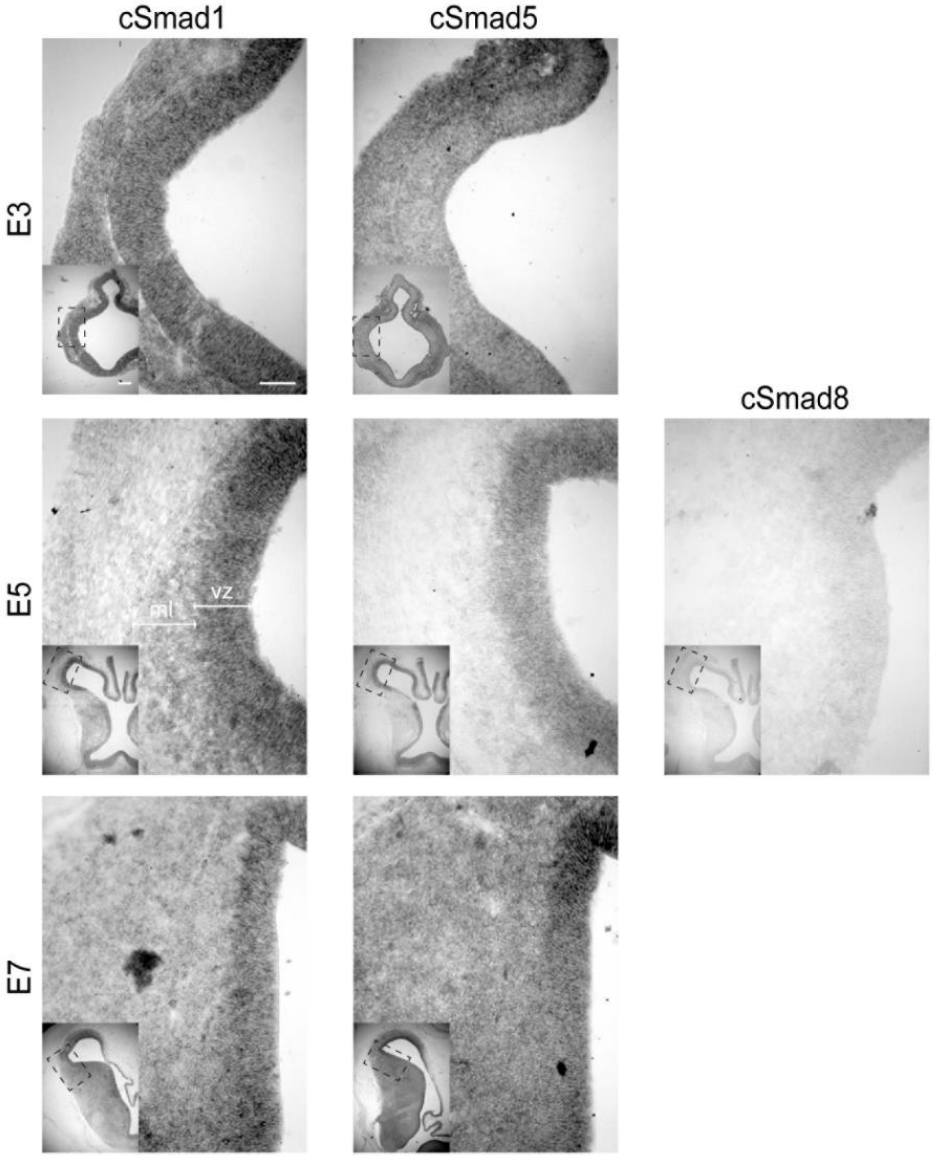

Extended Data Fig.2: Expression of cSmad1/5/8 during cortical neurogenesis in the chick.
Coronal sections showing *cSmad1, cSmad5 and cSmad8* expression as detected by *in situ* hybridization in the telencephalon of E3, E5 and E7 chick embryos. Scale bars: 50 µm. VZ: ventricular zone, ML: mantle layer.

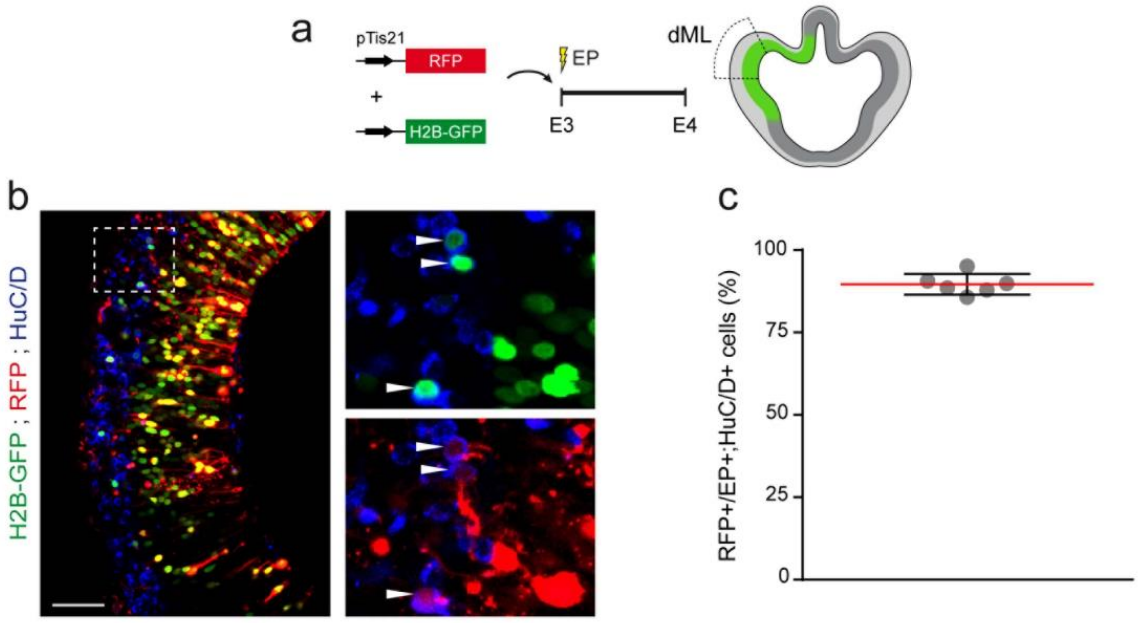

Extended Data Fig.3: Activity of the pTis21:RFP reporter in the chick developing cerebral cortex.
a, The activity of the pTis21:RFP reporter was assessed during cortical neurogenesis 24 hours after in ovo electroporation of the dorsal telencephalon of E3 chick embryos. **b**, Representative image of pTis21:RFP+ cells among the electroporated (H2B-GFP+) cells that differentiated into HuC/D+ neurons 24 hpe. **c**, The data represent the mean proportion of RFP+ cells among H2B-GFP+;HuC/D+ cells ± s.d obtained from n=6 electroporated embryos and show the individual values obtained for each embryo. Scale bars: 50 µm.

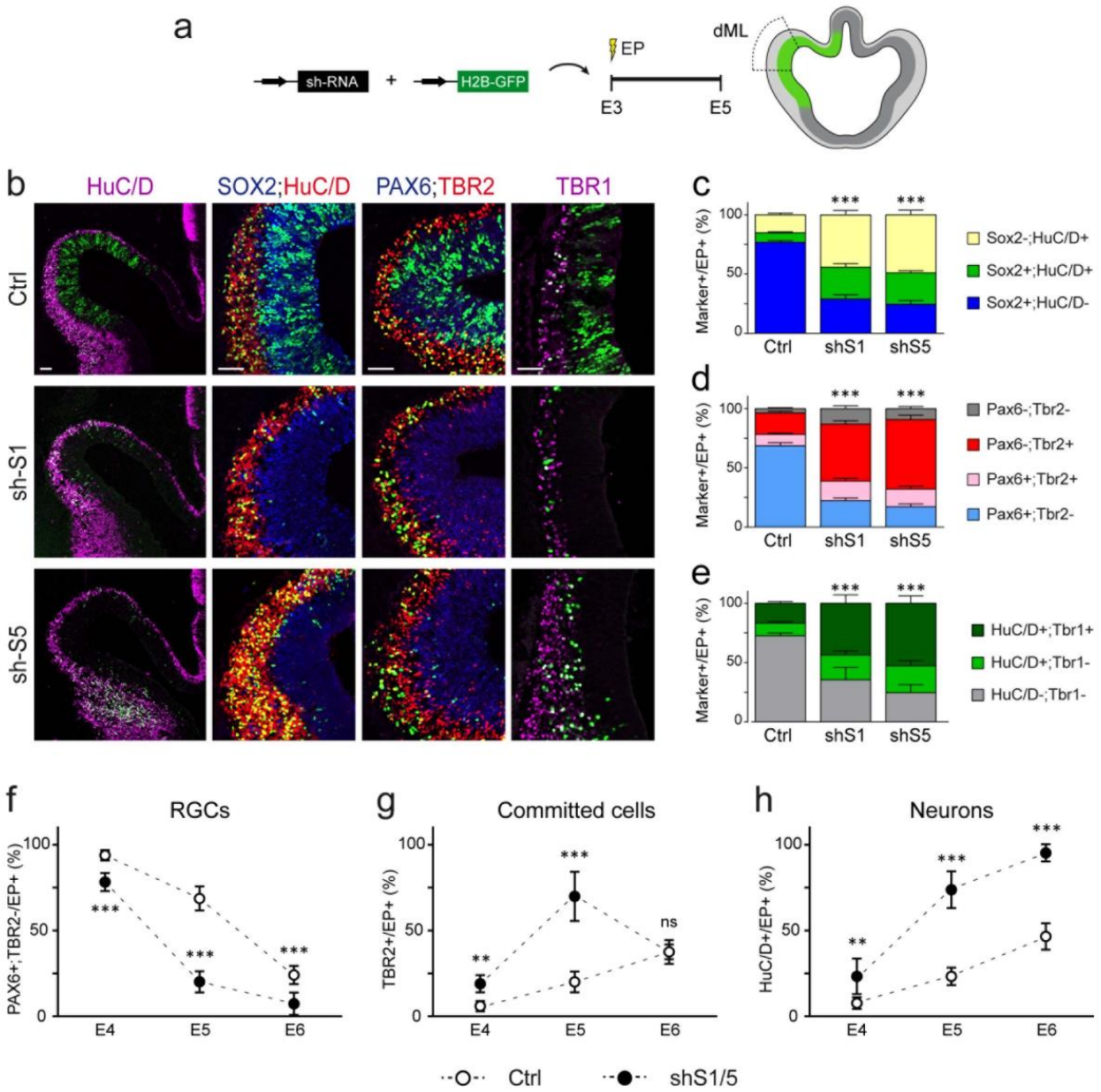

Extended Data Fig.4: inhibiting SMAD1/5 activity in chick cortical RGCs causes their premature exhaustion and progression towards neuronal commitment and differentiation.

a, The consequences of SMAD1/5 inhibition on chick cortical neurogenesis were assessed after *in ovo* electroporation (IOE) of shRNA plasmids targeting *cSmad1* (sh-S1) or *cSmad5* (sh-S5) in the dorsal telencephalon of E3 chick embryos together with a control plasmid producing H2B-GFP. **b**, Representative images of the electroporated (H2B-GFP+) cells that committed to the neuronal lineage (TBR2+) and differentiated into HuC/D+ and/or TBR1+ neurons 48 hours after IOE of sh-S1, sh-S5 or a control plasmid. **c-e,** The proportions of SOX2+/-;HuC/D+/- (**c**), PAX6+/-;TBR2+/- (**d**) and HuC/D+/;TBR1+/- (**e**) cells among electroporated (H2B-GFP+) cells were assessed 48 hours after IOE with sh-S1, sh-S5 or a control plasmid. The data represent the mean proportion ± s.e.m obtained from n embryos as follows: SOX2+/-;HuC/D+/- cells (control = 13, sh-S1= 8, sh-S5= 12), PAX6+/-;TBR2+/- cells (control = 8, sh-S1= 7, sh-S5= 5) and HuC/D+/;TBR1+/- cells (control = 9, sh-S1= 5, sh-S5= 6). Significance was assessed with a two-way ANOVA + Sidak's test. **f-h**, The proportions of PAX6+;TBR2- (RGCs, **f**), TBR2+ (committed cells, **g**) and HuC/D+ (Neurons, **h**) cells among electroporated (H2B-GFP+) cells were assessed 24 (E4), 48 (E5) and 72 (E6) hours after IOE with sh-S1/S5 or a control plasmid. The data represent the mean proportion ± s.d obtained from n embryos as follows: PAX6+;TBR2-/H2B-GFP+ cells (E4: control = 6, sh-S1/5= 16; E5: control = 8, sh-S1/5= 12; E6: control = 10, sh-S1/5= 9), TBR2+/H2B-GFP+ cells (E4: control = 6, sh-S1/5= 16; E5: control = 11, sh-S1/5= 14; E6: control = 10, sh-S1/5= 9) and HuC/D+/H2B-GFP+ cells (E4: control = 6, sh-S1/5= 13; E5: control = 13, sh-S1/5= 20; E6: control = 11, sh-S1/5= 9). Significance was assessed with a two-way ANOVA + Sidak's test.**P<0.01, ***P<0.001. Scale bars: 50 µm.

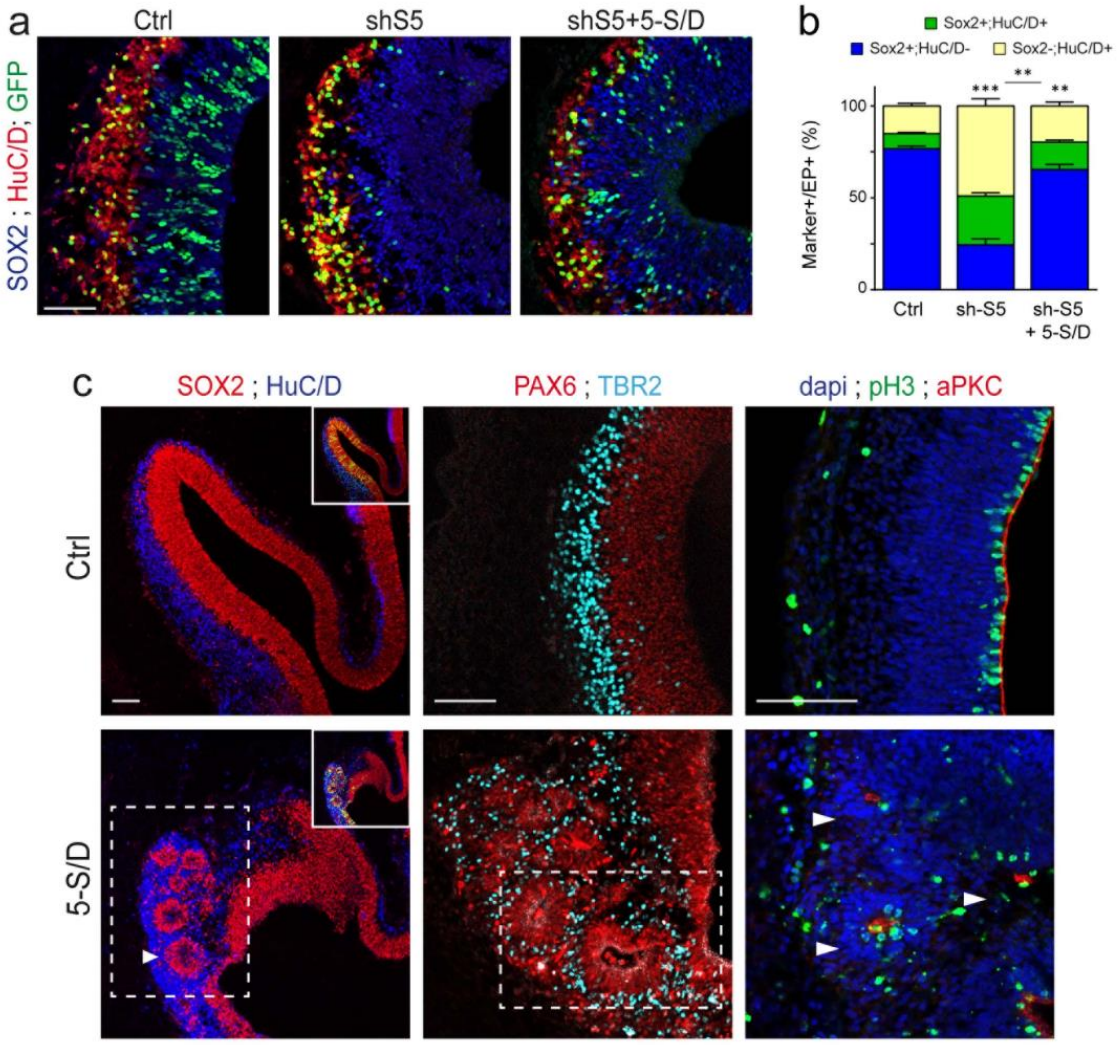

Extended Data Fig.5: SMAD5-S/D rescues the premature differentiation caused by sh-S5 during chick cortical neurogenesis and causes the abnormal generation of ectopic rosettes of cortical progenitors.

a, Representative images of electroporated (H2B-GFP+) cells that remained as SOX2+ cortical progenitors or differentiated into HuC/D+ neurons 48 hours after in ovo electroporation (IOE) of a control plasmid, or sh-S5 combined with a control plasmid or with the constitutively active SMAD5-S/D mutant (5-S/D). **b**, The proportion of SOX2+/-;HuC/D+/- cells among electroporated (H2B-GFP+) cells was assessed 48 hours after IOEin ovo electroporation with a control plasmid, or sh-S5 combined with SMAD5-S/D or with a control pCIG plasmid. The data represent the mean proportion ± s.e.m of SOX2+/-;HuC/D+/- cells among electroporated (H2B-GFP+) cells, assessed 48 hours after IOE and obtained from n embryos as follows: control = 13, sh-S5+pCIG = 12 and sh-S5+SMAD5-S/D = 8. Significance was assessed with a two-way ANOVA + Tukey's test. **P<0.01, ***P<0.001. **c**, Representative images showing that electroporation of the constitutively active SMAD5-S/D mutant (5-S/D) during early cortical neurogenesis in the chick can cause the abnormal generation of ectopic rosettes of SOX2+ cortical progenitors. The PAX6+ and TBR2+ cells forming these rosettes developed an ectopic apical-basal polarity, as revealed by immunostaining for the apical marker atypical PKC (aPKC), and divide mostly at the center of the rosettes (pH3+). Scale bars: 50 µm.

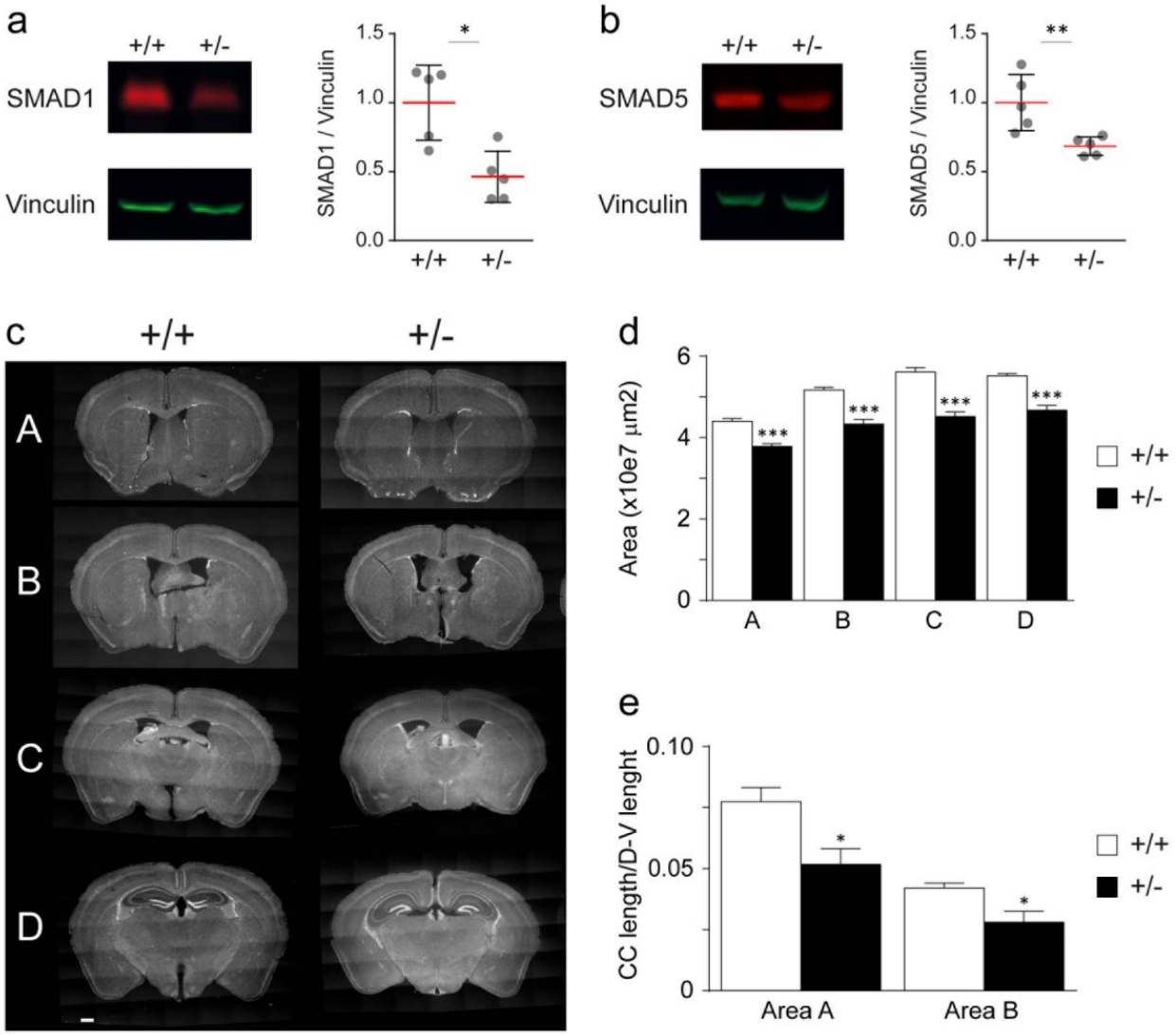

Extended Data Fig.6: Reduction in SMAD1/5 protein levels and brain size in the SmadNes mutant mice.
a-b, The levels of SMAD1 (a) and SMAD5 (b) proteins were assessed by Western blot in extracts obtained from telencephalons of E11.5 SmadNes mutant embryos (+/-) and control littermates (+/+), relative to the levels of Vinculin. The data represent the mean ratio ± s.d obtained from 5 mutant embryos and 5 control littermates. The mean values of individual embryos are shown. Significance was assessed with the non-parametric Mann-Whitney test. **c**, Representative images of the adult brain of SmadNes mutant mice (+/-) and their control littermates (+/+) in 4 different positions along the rostral-caudal axis (A to D, from rostral to caudal). **d**, The data represent the mean area ± s.e.m obtained from 3-5 embryos per genotype. Significance was assessed with a two-way ANOVA + Sidak's test. **e**, The thickness of the corpus callosum of the adult brain of SmadNes mutants and control littermates was measured in coronal sections in 2 different positions (A and B) along the rostral-axis, relative to whole dorsal-ventral (D-V) length. The data represent the mean ratio ± s.e.m obtained from 5 control and 3 mutant mice. Significance was assessed for each position with the non-parametric Mann–Whitney test. *P<0.05, **P<0.01, ***P<0.001. Scale bar: 500 µm.

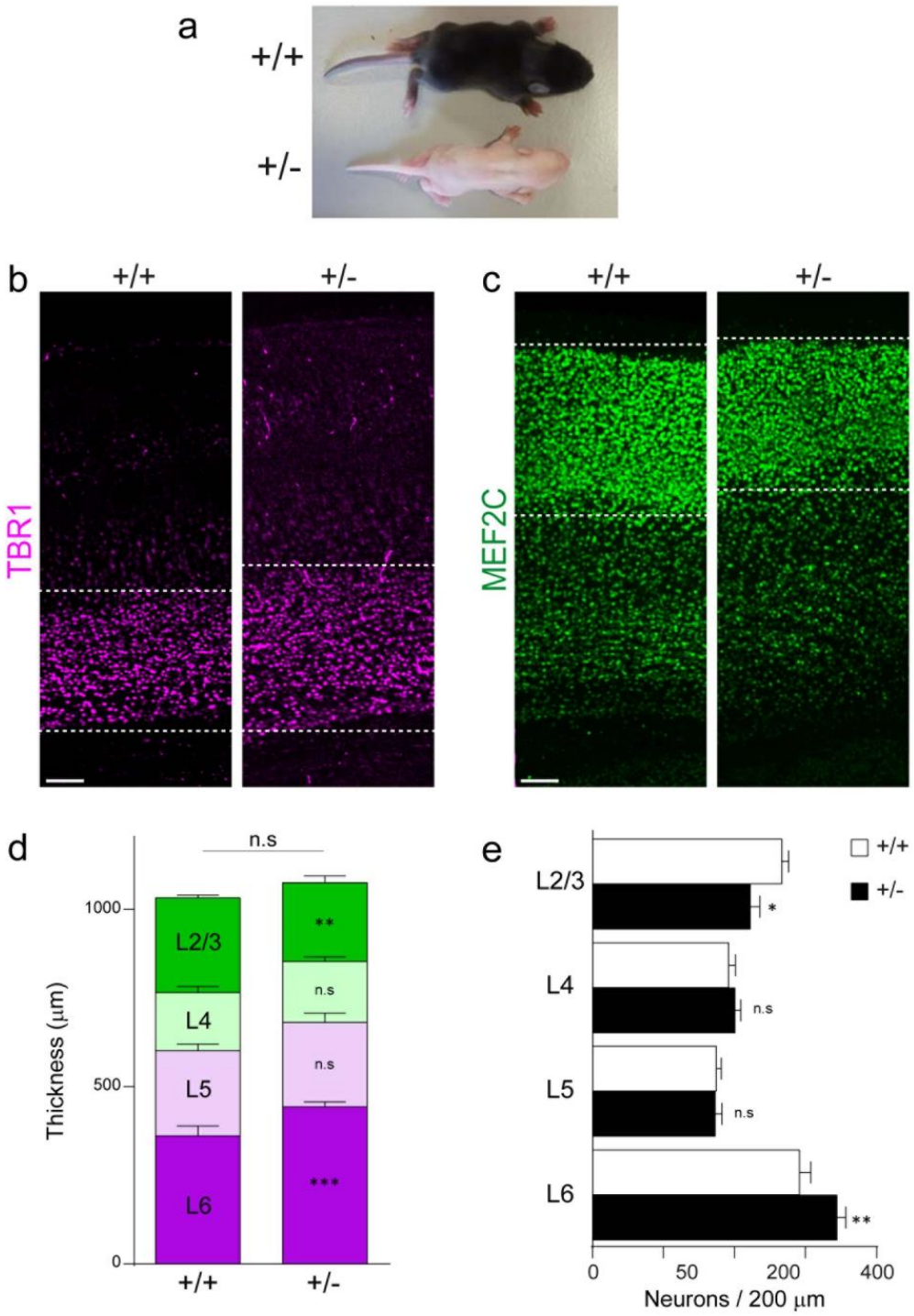

Extended Data Fig.7: The SmadNes mutants show reduced size and cortical alterations at P7.
a, SmadNes mutant mice (+/-) and their control littermates (+/+) at postnatal day 7 (P7). **b, c**, Representative images of the numbers and location of (**b**) early-born TBR1+ L6 and (**c**) late-born SATB2+ L4-2/3 projection neurons in the developing cerebral cortex of the SmadNes mutant pups and their control littermates. **d, e**, The data represent the mean thickness ± s.e.m (**d**) and mean number of neurons per layer in a 200 µm-wide radial column unit ± s.e.m (**e**) of the cerebral cortex of SmadNes mutants (n= 5) and control littermates (n= 6) at postnatal day P7. Significance was assessed with a two-way ANOVA + Sidak's test. For the total cumulated thickness (**d**), significance was assessed with the non-parametric Mann–Whitney test. *P<0.05, **P<0.01, ***P<0.001. Scale bar: 100 µm.

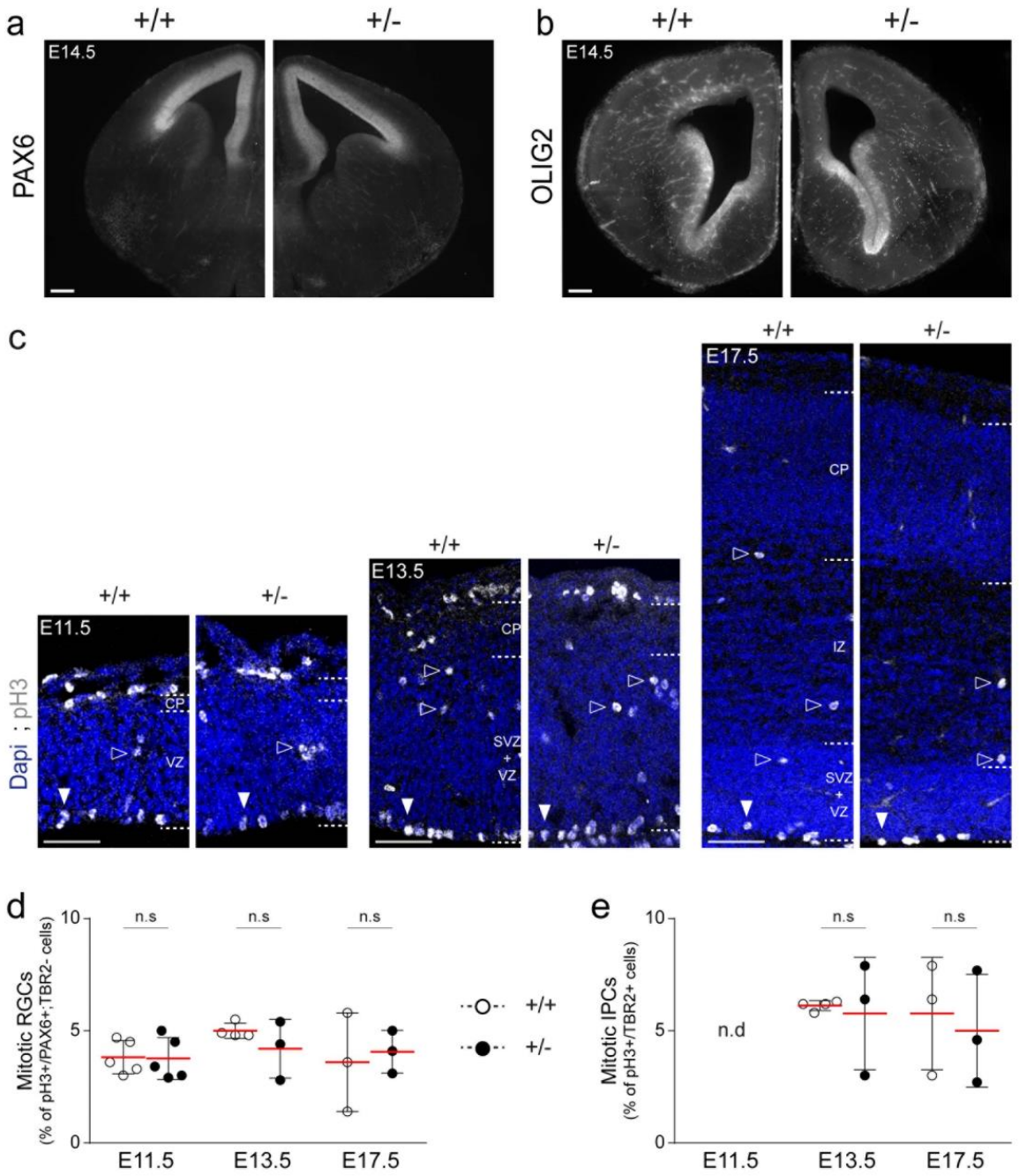

Extended Data Fig.8: Absence of patterning defects and cell cycle alterations in the cerebral cortex of SmadNes mutant embryos.
a, b, Coronal sections showing PAX6 (a) and OLIG2 (b) immunostaining in the telencephalon of E14.5 SmadNes mutant embryos (+/-) and control littermates (+/+). No obvious alteration in the expression domains of these pallial (PAX6) and sub-pallial (OLIG2) patterning markers was observed in the telencephalon of the SmadNes mutant embryos. **c**, Coronal sections showing apical (white arrowheads) and basal (black arrowheads) mitoses (pH3+) in the developing cerebral cortex of SmadNes mutant embryos (+/-) and control littermates (+/+) at E11.5, E13.5 and E17.5. **d,** The data represent the mean proportion of pH3+/PAX6+;TBR2- cells (mitotic RGCs) ± s.d counted in a 100 µm-wide radial column unit of the developing cerebral cortex of SmadNes mutant and control littermates embryos at E11.5 (Ctrl: 5 embryos, Mutant: 5 embryos), E13.5 (Ctrl: 4 embryos, Mutant: 3 embryos) and E17.5 (Ctrl: 3 embryos, Mutant: 3 embryos). **e**, The data represent the mean proportion of pH3+/ TBR2+ cells (mitotic IPCs) ± s.d counted in a 100 µm-wide radial column unit of the developing cerebral cortex of SmadNes mutant and control littermates embryos at E13.5 (Ctrl: 4 embryos, Mutant: 3 embryos) and E17.5 (Ctrl: 3 embryos, Mutant: 3 embryos). The normality was tested using the values of individual sections. The mean values of individual embryos are shown. Significance was assessed at each developmental stage with the two-sided unpaired t-test. NS: not significant. Nd: not determined. Scale bars, 100 µm (a, b), 50 µm (c). CP: cortical plate, IZ: intermediate zone, SVZ: sub-ventricular zone, VZ: ventricular zone.

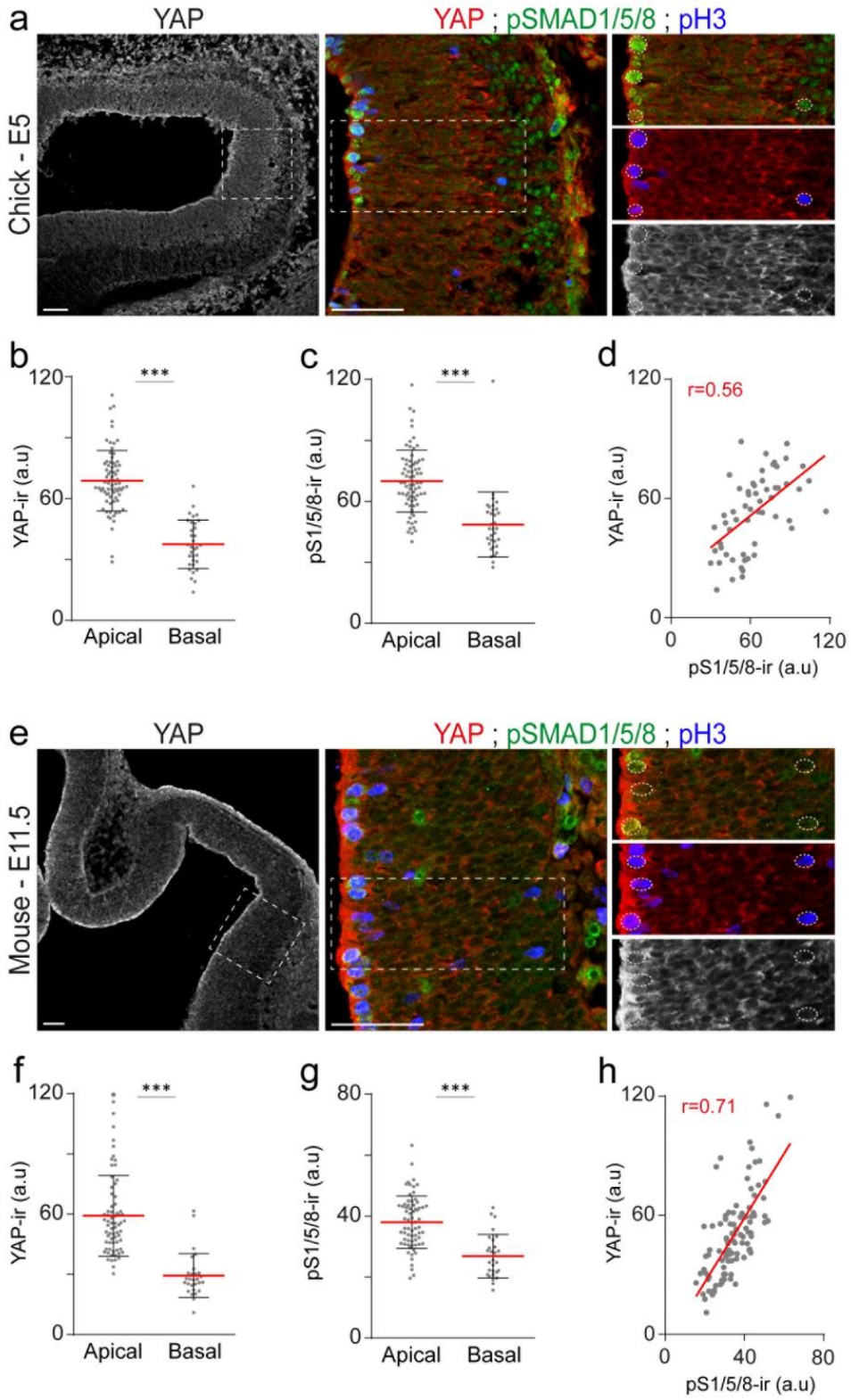

Extended Data Fig.9: Expression and activity of YAP during early corticogenesis in chick and mouse.
The expression and activity of YAP were assessed during early corticogenesis in chick (**a-d**) and mouse (**e-h**), relative to SMAD1/5 activity (revealed by pSMAD1/5/8 immunoreactivity). The intensity of endogenous YAP (**b, f**) and pSMAD1/5/8 (**c, g**) immunoreactivity was quantified in mitotic (pH3+) nuclei of apical and basal cortical progenitors obtained from chick E5 (n=3) and mouse E13.5 (n=3) embryos. The data represent the mean intensity ± s.d obtained from 74 apical divisions and 33 basal divisions (**b, c**), or 70 apical divisions and 28 basal divisions (**f, g**). The mean values of individual embryos are shown. Significance was assessed with the non-parametric Mann–Whitney test. **d, h**, The correlation between the intensity of endogenous pSMAD1/5/8 and YAP immunoreactivities was assessed by calculating the Pearson's correlation coefficient r. The mean values of individual embryos are shown. Significance was assessed with the two-sided unpaired t-test. ***P<0.001. Scale bar: 50 µm.

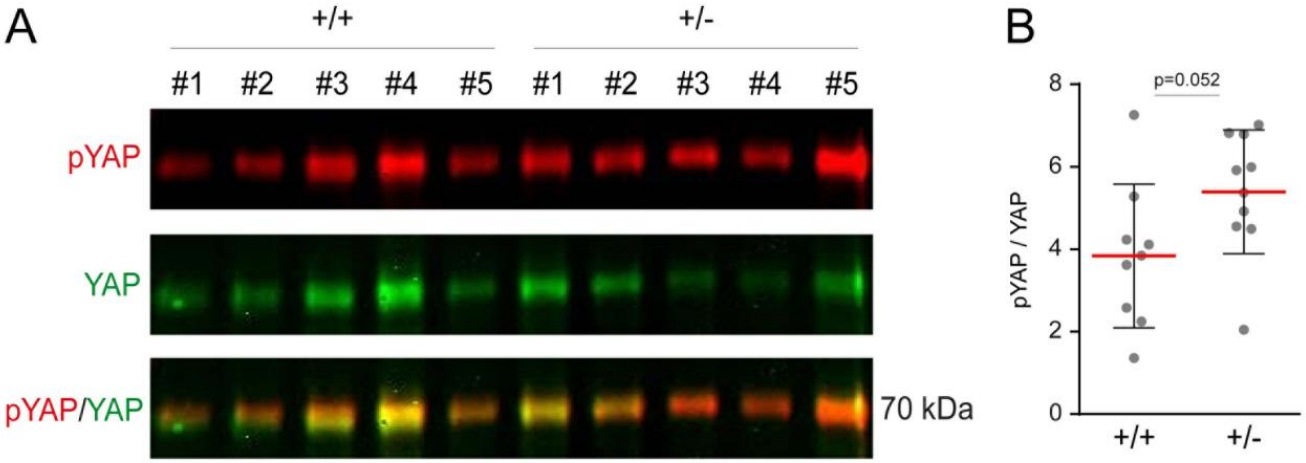

Extended Data Fig.10: The ratio pYAP/YAP is increased in the telencephalon of E11.5 SmadNes mutant embryos.
a, Western blot detection of the levels of the form of YAP phosphorylated at Serine 123 (pYAP) and total YAP in extracts obtained from telencephalons of E11.5 SmadNes mutant embryos (+/-) and control littermates (+/+). **b**, The levels of pYAP and total YAP proteins were quantified in extracts obtained from telencephalons of E11.5 SmadNes mutant embryos (+/-) and control littermates (+/+). The data represent the mean ratio ± s.d obtained from 10 mutant embryos and 9 control littermates of two different litters. The dots represent values of individual embryos. Significance was assessed with the two-sided unpaired t-test.